Investigating the role of chronic OPA1 loss in muscle stem cell maintenance and activity

Olivia Sommers

A thesis submitted to the University of Ottawa in partial fulfillment of the requirements for the integrated Honours Bachelor of Science in Translational & Molecular Medicine and Master's of Science in Biochemistry degrees

Department of Biochemistry, Microbiology, and Immunology
Translational & Molecular Medicine Program
Faculty of Medicine
University of Ottawa

ABSTRACT

Adult muscle stem cells (MuSCs) play a crucial role in tissue regeneration, yet the mechanisms governing their dysfunction and depletion during aging remain unclear. However, during aging, regulators of mitochondrial dynamics, a key regulator of MuSC activity and fate, decline in expression. This loss of mitochondrial fission and fusion modulators has been associated with premature aging phenotypes in whole muscle and MuSC dysregulation with age. To date, how mitochondrial dynamics contribute to senescent and aged-like phenotypes in MuSCs has not been fully described. Our lab has previously implemented a Pax7CreERT2 inducible system to conditionally knock-out the mitochondrial fusion protein OPA1 specifically within MuSCs (OPA1-KO) and found that with chronic loss of OPA1, MuSCs have enhanced activation kinetics, significant proliferation defects, and evidence of mitochondrial dysfunction. In this current work, we sought to address the role of chronic OPA1 loss in MuSCs, particularly in the contexts of aging and senescence. We found that with chronic loss of OPA1, MuSCs accumulate biomarkers of senescence, experience cell cycle dysregulation at the transcriptional level, and have a dysregulated metabolome. However, the proliferative defects associated with chronic OPA1 ablation may be partially mitigated via supplementation of exogenous metabolites. Notably, at 9 months of OPA1 loss, the phenotype of MuSC dysfunction was found to progress to the extent of stem cell depletion basally. Further, whole-muscle defects were observed at this time, including the onset of a muscle wasting phenotype (with a reduction in the myofiber cross-sectional area and the number of myonuclei per myofiber) and increased fatiguability of the muscle. These findings suggest that mitochondrial dynamics are a critical regulator of MuSC activity and maintenance in an aging context, and that whole muscle health during aging is dependent on the presence of functional MuSCs. This research offers novel therapeutic insight that may be leveraged to improve muscle stem cell health and function with age.

KEYWORDS: Muscle Stem Cell, Mitochondrial Dynamics, OPA1, Cellular Senescence, Skeletal Muscle, Aging, Cell Cycle, Metabolism

Acknowledgements

I would like to firstly express my deepest gratitude to my supervisor, Dr. Mireille Khacho, for her invaluable guidance, kindness, and encouragement throughout the course of this project. She has provided me with numerous exciting opportunities throughout my time in her lab and I am extremely grateful. Her insightful feedback and expertise have been instrumental in shaping this work, and her unwavering support both academically and personally means so much to me. To me, she is the definition of what a great scientist and leader should look like, and I hope to continue learning more from her in the years to come.

I am also sincerely grateful to my thesis advisory committee members, Dr. Yan Burelle and Dr. Luca Pellegrini, for their mentorship, encouragement, and constructive feedback, which have greatly enriched my research.

A special thank you to my lab members and colleagues, Matt Triolo, Steven Wade, Kayla Ferguson, Rholls Tomsine, Edward Gardner, Nikita Larionov, and Pamela Khacho, for their support, technical assistance, and enriching (if not highly entertaining) discussions. I am grateful to have spent my time at the Khacho Lab working alongside you all, and I couldn't have asked for a better team to be a part of.

On a personal note, I am also deeply thankful to my parents and my close friends for their unwavering support and patience throughout this process. They have been an anchor for me, especially during the challenging times associated with graduate studies. Finally, to all those who, in one way or another, have contributed to the completion of this thesis—thank you.

Table of Contents

Abbreviations

ADP	Adenosine Diphosphate
ATP	Adenosine Triphosphate
BSA	Bovine Serum Albumin
CalcR	Calcitonin Receptor
CCND1	Cyclin D1
CD34	Cluster of Differentiation 34
CD47	Cluster of Differentiation 47
CDK4	Cyclin-Dependent Kinase 4
CDK6	Cyclin-Dependent Kinase 6
CPEB4	Cytoplasmic Polyadenylation Element Binding Protein 4
CSA	Cross-Sectional Area
CTX	Cardiotoxin
DDR	DNA Damage Response
DNA	Deoxyribonucleic Acid
DPI	Days Post-Injury
DRP1	Dynamin Related Protein 1
DSB	Double-stranded Breaks
EDL	Extensor Digitorum Longus Muscle
ELISA	Enzyme-Linked Immunosorbent Assay
eMHC	Embryonic Myosin Heavy Chain
ER	Endoplasmic Reticulum
ETC	Electron Transport Chain
FBP1	Fructose-Biphosphatase 1
FBS	Fetal Bovine Serum
FGF-21	Fibroblast Growth Factor 21
Fis1	Mitochondrial Fission Protein 1
GSH	Reduced Glutathione
GTP	Guanosine Triphosphate
H&E	Hematoxylin & Eosin

H3K27	Histone H3 Lysine-27
H3K4ac	Histone H3 Lysine-4 Acetylation
H3K4me1	Histone H3 Lysine-4 Monomethylation
H3K9	Histone H3 Lysine-9
HDAC1	Histone Deacetylase 1
HGF	Hepatocyte Growth Factor
IL-6	Interleukin-6
IMM	Inner Mitochondrial Membrane
Ki67	Antigen Kiel 67
KO	Knockout
L-OPA1	Long Form of Optic Atrophy 1
LC-MS/MS	Liquid Chromatography-Mass Spectrometry
MAPK	Mitogen-Activated Protein Kinase
MFN1	Mitofusin 1
MFN2	Mitofusin 2
MHC	Myosin Heavy Chain
MHC I	Myosin Heavy Chain I
MHC IIa	Myosin Heavy Chain IIa
MHC IIb	Myosin Heavy Chain IIb
MHC IIx	Myosin Heavy Chain IIx
MID49/51	Mitochondrial Dynamics Protein 49 and 51
MMP3	Matrix Metalloproteinase-3
MRF-4	Myogenic Regulatory Factor-4
mTOR	Mammalian Target of Rapamycin
MuSC(s)	Muscle Stem Cell(s)
Myf5	Myogenic Factor 5
MyoD	Myoblast Determination Protein
MyoG	Myogenin
OCR	Oxygen Consumption Rate
OCT	Optimal Cutting Temperature
OMM	Outer Mitochondrial Membrane

OPA1	Optic Atrophy 1
ORO	Oil Red O
OXPHOS	Oxidative Phosphorylation
Pax7	Paired Box 7
PBS	Phosphate Buffered Saline
PFA	Para-Formaldehyde
pS6	Ribosomal Protein S6
Rb	Retinoblastoma Protein
RNA	Ribonucleic Acid
RNA-seq	RNA Sequencing
ROS	Reactive Oxygen Species
RT-qPCR	Real Time Quantitative Polymerase Chain Reaction
S-OPA1	Short Form of Optic Atrophy 1
SAHF	Senescence-Associated Heterochromatin Foci
SAMD	Senescence-Associated Mitochondrial Dysfunction
SASP	Senescence-Associated Secretory Phenotype
TA	Tibialis Anterior Muscle
TAM	Tamoxifen
TCA	Tricarboxylic Acid Cycle
TNF	Tumor Necrosis Factor
UPR	Unfolded Protein Response
UTP	Uridine-5-Triphosphate
γ-H2AX	Gamma H2A Histone Family Member X

List of Tables

List of Figures

Chapter 1: Introduction

1.1 Overview of skeletal muscle

Skeletal muscle is a major tissue of the human body, making up 40% of body mass[1] and contributing to numerous vital processes including locomotion, respiration, and whole-body metabolism[1–4]. Two major functions of the skeletal muscle are force generation and tissue regeneration. Skeletal muscle is organized in groups of muscle fibers (also referred to as myofibers) into units called fascicles, which are wrapped in connective tissue called the endomysium, made of the reticular and basal laminas[1,5–7]. Myofibers are post-mitotic, multinucleated cells comprised of numerous myofibrils formed by repeating units known as sarcomeres[8–12]. Sarcomeres are arranged in series of thick filaments (myosin) and thin filaments (actin) along with other regulatory proteins like troponin, which bind and pull against one another to allow for contraction[12–21]. In this way, the structural organization of skeletal muscle gives rise to its contractile functions. Within the skeletal muscle, there are a host of cell populations beyond the myofibers themselves. For instance, motor neurons, fibroblasts, fibroadipogenic progenitors, endothelial cells, and immune cells are other important populations which have functional roles within the skeletal muscle[22–28]. One essential population are the muscle stem cells, which are essential for the regenerative capacity of the muscle[5,6,23,29–31].

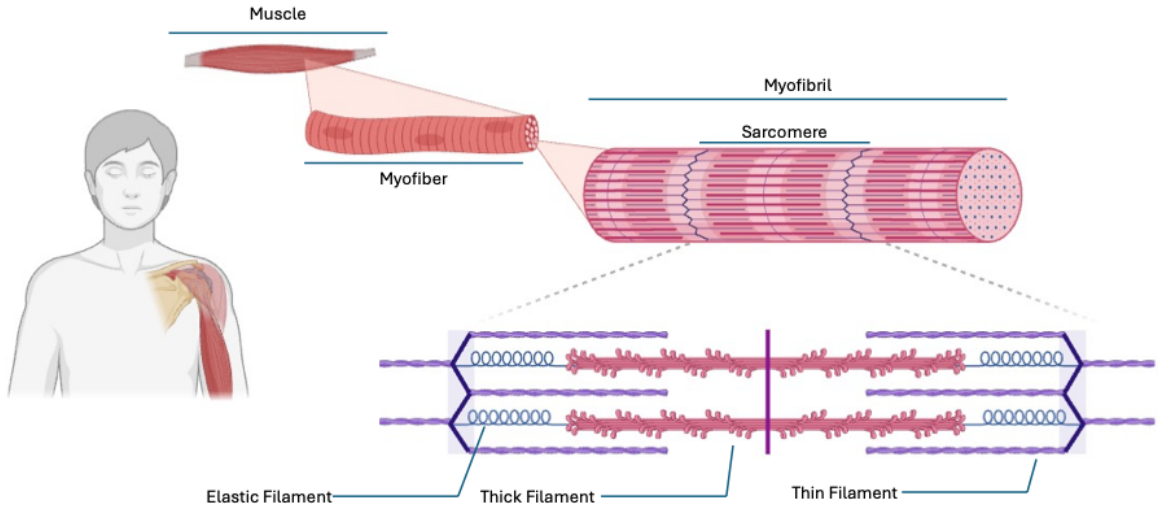

Figure 1. Overview of the hierarchical structure of skeletal muscle. The anatomy of skeletal muscle allows for its function in force generation. Briefly, muscle is comprised of myofibers bundled into fascicles by the endomysium. Myofibers are comprised of myofibrils, which are arranged into repeating units of sarcomeres. Sarcomeres contain a variety of filaments, including thick (myosin), thin (actin), and elastic (titin) filaments,

along with regulatory proteins, which pull against one another to allow for muscle contraction. Figure made in part with *BioRender*.

1.2 Overview of adult muscle stem cells

Adult muscle stem cells (MuSCs; also known as satellite cells) are the resident stem cell population of skeletal muscle that give rise to its regenerative capacity, allowing for the maintenance of muscle mass and quality throughout the lifespan[6,7,32]. During homeostasis, MuSCs exist in a niche beneath the basal lamina of mature muscle fibers in a state of quiescence[33,34]. This niche provides structural support and relays cellular signals to and from the MuSCs and other muscle cell populations[6,33,34]. As such, MuSCs exist in an environment in which they can readily respond to intrinsic and extrinsic signals to execute their major functions. As stem cells, MuSCs bare the two major abilities of committing to myogenic differentiation to allow for tissue repair and regeneration, or self-renewing, which maintains the stem cell pool[6,33,34]. Following an activation stimulus such as injury, MuSCs exit quiescence and enter a G_{alert} state, become activated, and undergo the fate decisions of committing to the myogenic program, giving rise to myogenic progenitors, or self-renewing and returning to a state of quiescence[35–38]. Due to their contribution for the regeneration of whole skeletal muscle, MuSCs have been studied in the context of aging in order to improve muscle maintenance across the lifespan.

1.3 Overview of myogenesis

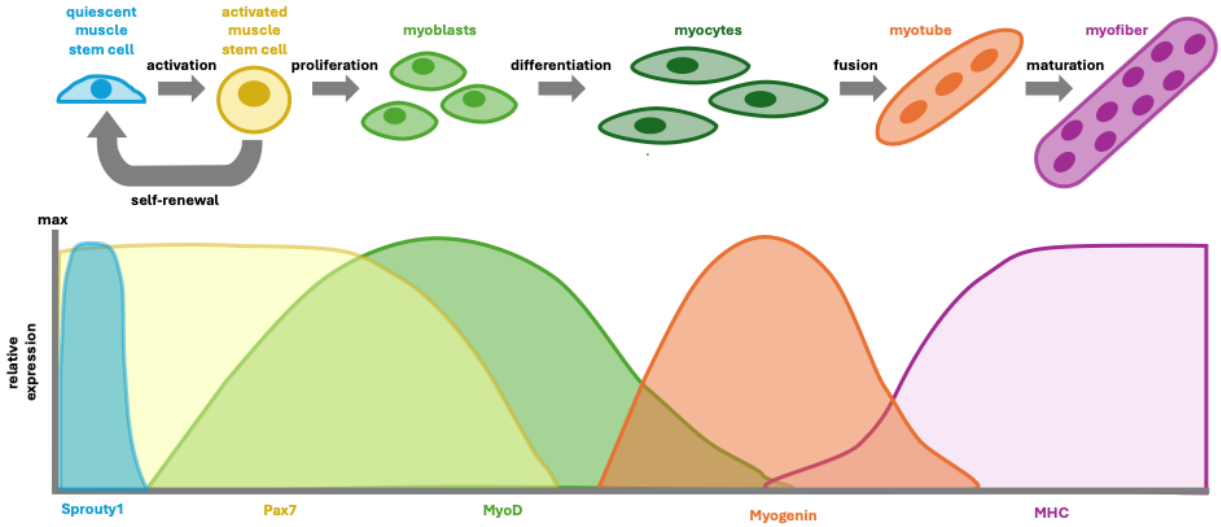

Figure 2. Overview of the myogenic program. During homeostasis, muscle stem cells exist in a quiescent state denoted by high Pax7 expression. They can be activated by a stimulus such as injury and upregulate MyoD. Activated muscle stem cells can commit to differentiation, in which they upregulate the myogenic regulatory factor myogenin (MyoG), fuse into myotubes, and ultimately mature into MHC-expressing myofibers. Alternatively, muscle stem cells

can self-renew to a state of quiescence, in which they re-upregulate Pax7 and return to dormancy. Figure adapted from Schmidt *et al.* (2019) *Cellular and Molecular Life Sciences*.

1.3.1 Muscle stem cell quiescence and activation

Under physiological conditions, MuSCs reside in a reversible state of dormancy at the G_0 phase of the cell cycle, known as quiescence[39,40]. Quiescence is a non-proliferative state that preserves the stemness of the MuSCs, maintains the stem cell pool, and is tightly regulated by intrinsic and extrinsic signals[41]. Many features of the quiescent state enable MuSCs to remain dormant. For instance, quiescent MuSCs have reduced metabolic activity and a reliance on fatty acid oxidation, exhibit relatively lower levels of reactive oxygen species (ROS), minimal protein synthesis, and repressed transcriptional activity[42,43]. Quiescent MuSCs express the transcription factor Pax7, a widely used marker in the field of regenerative medicine to label MuSCs. Their transcriptional profile is distinct from other states such as activation, and includes high expression of factors including CD34, Sprouty1, Calcitonin Receptor (CalcR), Integrin α7, and Notch Receptor, among others[44–48]. Quiescence is a graded physiological state, ensuring fine-tuned control that prevents precocious activation and allows MuSCs to respond appropriately to different stimuli. There is a distinct difference between the traditional G_0 quiescent state and the G_{alert} state, in which MuSCs are primed for activation[42,49]. G_{alert} MuSCs enhance their transcriptional activity and their mitochondrial metabolism, and also have an enlarged, less squamous cell shape compared to G_0 MuSCs[42,50]. In a physiological setting, muscle injury serves as a potent stimulator of activation, preparing quiescent MuSCs to enter the cycle and progress through the myogenic differentiation program[6,46,51]. The transition towards activation is associated with notable changes in gene expression, including expression of the myogenic differentiation factors *MyoD* and *Myf5* and positive cell cycle modulators, as well as a shift towards a more glycolytic metabolic state[50,52–54]. One signaling pathway of interest that regulates the transition from quiescence to activation is the mammalian target of rapamycin (mTOR) pathway[42,50]. As MuSCs enter an activated state, they enhance expression of the mTOR intermediate, pS6[42,50]. Importantly, stimulation of the mTOR pathway through genetic or pharmacological means is sufficient to promote the transition from G_0 to G_{alert} states in MuSCs[42,50], and conversely, inhibition of the mTOR pathway is sufficient to maintain a G_0 phenotype[50].

1.3.2 Fate decisions: commitment or self-renewal

Activated MuSCs enter the cell cycle, are primed for proliferation, and undergo the fate decisions of either committing to myogenic differentiation to give rise to myogenic progenitors or self-renewing to a state of quiescence[55–57]. In the self-renewing population, there is a coordinated suppression of myogenic regulatory factors like MyoD, an upregulation of Pax7 and Sprouty1 to terminate the differentiation program, and a reintroduction of pathways involved in quiescence such as Notch signaling[29,35,51,58,59]. Self-renewal is a critical process that ensures the long-term maintenance of the stem cell pool and the ability to contribute to muscle regeneration across the lifespan. Notably, in degenerative diseases and during aging, imbalances in fate decisions occur in which commitment is favoured at the expense of self-renewal, leading to depletion of the quiescent MuSC pool and contributing to a phenotype of defective muscle regeneration[56,57,60,61]. During commitment, Pax7 remodels the chromatin landscape in MuSCs, promoting the recruitment of the histone marks H3K4me1 and H3K4ac to increase chromatin accessibility[62] and also promotes DNA looping to activate the transcription of MyoD[63]. Importantly, expression of MyoD does not occur during MuSC quiescence; it becomes upregulated during the proliferative stage, and as committed MuSCs progress through the differentiation program, its expression declines[64,65]. Myoblasts differentiate into myocytes and undergo fusion into myotubes, regulated by MyoG and MRF-4[66–69]. The process of fusion results in the generation of new myofibers that transiently express embryonic myosin heavy chain (eMHC)[70,71], but which develop and express adult isoforms of MHC[70–72].

1.4 Aging skeletal muscle

During aging, skeletal muscle undergoes a variety of changes that collectively result in a decline of muscle mass, strength, and function, also referred to as sarcopenia[73,74]. Sarcopenia drastically impacts the quality of life in older individuals, reducing their mobility and increasing their risk for falls, fracture, and death[60,75]. This progressive disorder begins as young as 40 years old and by the age of 70, approximately 40% of muscle strength is lost[76,77]. Some of the established changes which occur in aging skeletal muscle that contribute to the sarcopenic phenotype are the onset of muscle atrophy program, which reduces the cross-sectional area of myofibers[78–80], loss of fast-twitch myofibers[74,79], muscle denervation[81,82], and metabolic dysregulation or oxidative stress within the myofibers[83–85]. Age-related changes within the skeletal muscle, such as persistent low-

grade inflammation, can lead to both muscle atrophy and MuSC depletion, with negative consequences on muscle regeneration[86]. For instance, in geriatric mice, IL-6 levels are elevated after injury and have been shown to stimulate the IL-6-Jak2-Stat3 signaling axis and induce MuSC exhaustion as well as muscle atrophy[87,88].

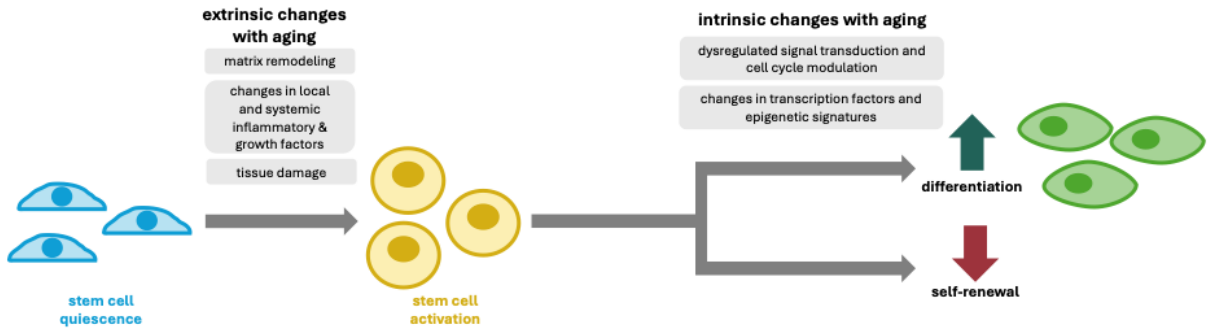

Figure 3. Intrinsic and extrinsic changes with aging influence muscle stem cell fate and maintenance. Extrinsic changes associated with aging, such as inflammatory cytokines in the circulation or in the local environment, can stimulate activation of muscle stem cells. These extrinsic change converge to induce intrinsic changes in muscle stem cell signaling which alter the fate decisions of muscle stem cells, promoting differentiation at the expense of self-renewal. With aging and senescence, cumulative insults lead to the loss of homeostasis, depleting the quiescent muscle stem cell pool.

1.5 Aging muscle stem cells

A balance must be struck for MuSCs between residing in a quiescent state and retaining the ability to respond to activation cues such that skeletal muscle function and regeneration can be maintained. Cell-intrinsic and -extrinsic factors associated with aging, such as changes in cytokines and growth factors in the local environment, or differential regulation of cell cycle modulators can impair muscle regeneration[34,51,89]. This is often achieved by increasing the propensity of MuSCs to activate and commit to differentiation at the expense of self-renewal, ultimately limiting the number of functional MuSCs available to respond to future insult[31,87,88,90,91].

In transplantation models, MuSCs from older donors show defective self-renewal and limited expansion[31,87,88,91]. Further, aged MuSCs have defects in engrafting in the damaged tissues of secondary young recipients[31,87,92]. Thus, in addition to the changes associated with aging in the whole skeletal muscle, aged MuSCs have intrinsic defects that cannot be restored by rejuvenating their environment. An example of a stem cell defect associated with age in MuSCs is their loss of stemness. During aging, protein expression of the quiescence markers CD34 and Pax7 is downregulated in MuSCs[93]. Further, RNA-sequencing (RNA-seq) analysis shows that with age,

quiescent MuSCs downregulate Notch signaling-associated genes, including Hey1/L, Hes1, and collagen V[93]. Aging MuSCs also show signs of dysregulated metabolism and mitochondrial dysfunction, particularly through a decline in tricarboxylic acid (TCA) cycle- and oxidative phosphorylation (OXPHOS)-related protein expression, dramatic reductions in basal and maximal oxygen consumption rates (OCRs), and a decline in mitochondrial ATP generation[93].

Numerous signaling cascades, such as the p38α -MAPK signaling axis and $p16^{Ink4a}$-Rb cell cycle inhibition, are stimulated by factors such as inflammation which are associated with aging[31,88] and converge on a shared set of cell cycle kinases and myogenic factors like MyoD[92]. Members of these axes can alter MuSC activation and fate decisions or limit cell cycle progression, effectively limiting the number of MuSCs available for regeneration. For instance, TNF-mediated inflammation stimulates p38α-mediated chromatin repression at the promoter of Pax7, a marker of quiescent MuSCs[94–96]. Exhaustion of the stem cell pool can also be achieved through cellular senescence[93].

1.6 Cellular senescence

Cellular senescence describes the irreversible arrest within the G_1/S or G_2/M phases of the cell cycle, often in response to damaging stimuli[97]. In this way, senescence is distinct from the reversible G_0 phase growth arrest associated with quiescence (described above). The early work of Hayflick and Moorhead was the first to suggest a potential relationship between senescence and aging[76], but it is now known that senescent cells exponentially accumulate in aged tissues and appreciated that senescence is both a hallmark and driver of the aging phenotype[97,98].

While cellular senescence has both beneficial and deleterious effects, it is typically known for its deleterious roles, particularly when excessive or aberrant accumulation of senescent cells occurs[99,100]. The context and system in which the senescence program is initiated plays a key role in determining its effects; for instance, while it has been suggested that senescence can serve as a safeguard against tumorigenesis, such as in in prostate cancer[101,102], it has also been shown to promote tumorigenesis in liver cancer via loss of FBP1[103]. Ultimately, the phenotype of cellular senescence is highly heterogeneous across cell and tissue types, and the accumulation of senescent cells negatively affects the regenerative capacity of many different tissue types[104], contributing to the aging phenotype.

There is a diverse range of triggers for cellular senescence that have been described in a variety of tissues and organisms, including telomere shortening, DNA damage, oncogene dysregulation, oxidative stress, mitochondrial dysfunction, epigenetic dysregulation, and paracrine senescence[104–110]. To date, there are no established universal mechanisms associated with cellular senescence that are conserved across cell or tissue types[111]. This speaks to the complexity and heterogeneity of the senescence program and presents challenges in identifying senescent populations[89]. The current standard in the field is to measure multiple hallmarks of senescence within the same sample to determine whether that population is senescent[111]. As such, a number of different signalling pathways or other features associated with cellular senescence have become an important tool to identify senescent populations. For instance, the unique secretome of senescent cells, referred to as the senescence-associated secretory phenotype (SASP), contains pro-inflammatory and pro-fibrotic factors such as interleukins and matrix metalloproteases capable of inducing senescence in nearby cycling cells[89,112]. Additionally, during senescence, cells become unresponsive to factors that typically stimulate proliferation, including growth factors and mitogenic signals[113]. For instance, mTOR and other nutrient-sensing pathways alter cell cycle progression: during senescence, persistent activation of mTOR allows for stable cell cycle arrest[114], whereas the arrest associated with quiescence is enabled with inhibition of mTOR[50,114].

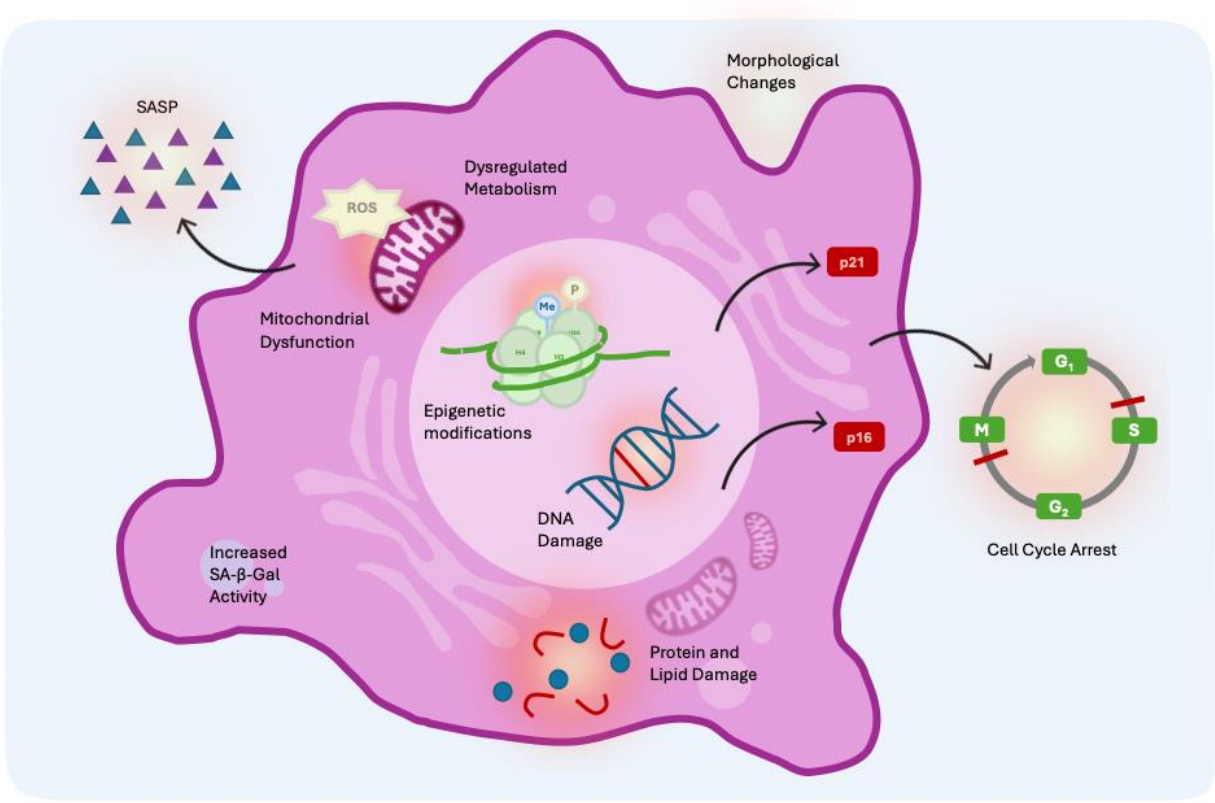

Figure 4. Characteristics of senescent cells. The senescent phenotype has diverse features. These are illustrated in the figure, and include irreversible cell cycle arrest, dysregulated metabolism, DNA, protein, and lipid damage, mitochondrial dysfunction, epigenetic modifications, excessive accumulation of reactive oxygen species (ROS), enhanced SA-β-Gal (senescence-associated β-galactosidase) activity, the SASP (senescence-associated secretory phenotype), and morphological changes.

1.6.1 Senescent muscle stem cells

While the mechanism of sarcopenia is not entirely understood, because age-dependent deficits in tissue repair are correlated with stem cell dysfunction[115–118], several studies have suggested that senescence of MuSCs plays a role[87,92,93,119–121]. Importantly, it has been shown that during aging, quiescent MuSCs in resting skeletal muscle can undergo irreversible cell cycle arrest and transition to a state of senescence[87,121].

While there are diverse causes of cellular senescence in MuSCs, there are conserved features and markers in which they exhibit. For instance, senescent MuSCs possess the characteristic pro-inflammatory and pro-fibrotic SASP, with deleterious effects on muscle regeneration and on the cell cycle progression of other MuSCs and cycling cells within the local environment. Porpiglia *et al*. show that senescent MuSCs accumulate CD47 at the cell surface via alternative polyadenylation, and through a paracrine signaling loop, experience impaired proliferation and impaired muscle regeneration[89]. Notably, while there is a role for the transient

upregulation of particular SASP components like pro-inflammatory cytokines in promoting muscle repair, the persistent expression of SASP factors is deleterious and impairs the regeneration program in an aging context[92]. To improve the regenerative capacity of aged skeletal muscle, senescent MuSCs must be cleared. Baker *et al.* show that in geriatric mice, chronic expression of $p16^{Ink4a}$ is associated with muscle regeneration defects and an accumulation of senescent MuSCs[122,123]. However, muscle regeneration could be improved via the conditional ablation of the senescent population[123].

Mechanisms which transcriptionally dictate MuSC proliferation have been highlighted in the literature. Modes of interest in the context of cellular senescence involve the coordinated, active repression of myogenic differentiation genes and of genes which negatively regulate the cell cycle. For instance, HDAC1 can interact with MyoD to repress the MyoD-dependent transcription of p21, an inhibitor of the G_1/S transition[124]. p21 is a conserved marker of senescence and is upregulated in senescent MuSCs[125]. Interestingly, Englund *et al.* have recently shown that overexpression of p21 in mice leads to signs of muscle pathology, including atrophy and fibrosis, as well as markers of senescence in the muscle, including DNA damage, mitochondrial dysfunction, and presence of the SASP[126]. NELF-mediated inhibition of p53 is also required for muscle regeneration to enable MuSC proliferation and expansion post-injury[127]. Interestingly, p53 repression and defective spindle assembly in aged skeletal muscle leads to a depletion of the MuSC pool, a process referred to as "mitotic catastrophe" by Liu *et al.*[128]. Relatedly, Zeng *et al.* show that CPEB4, a target of p53, mediates mitochondrial dysfunction and MuSC senescence at the translational level by targeting mRNA transcripts[93]. This axis may be a therapeutic target for treating age-related muscle wasting by targeting mitochondrial metabolism. Additionally, loss of Cyclin D1 is often observed in aged MuSCs and leads to the suppression of TGFβ-SMAD3 signaling, reported to impair MuSC proliferation through the upregulation of CDK inhibitors[119,129].

1.7 Overview of mitochondria

1.7.1 Mitochondrial metabolism

Mitochondria are highly dynamic double-membrane organelles, important for both their bioenergetic capacity and their cell signaling functions. The key bioenergetic functions of mitochondria revolve around energy production and metabolic regulation. One major contribution of the mitochondria is their generation of adenosine triphosphate (ATP) via OXPHOS. This occurs

in the electron transport chain (ETC) in which electrons are shuttled between ETC complexes, generating a proton motive force that ultimately drives ATP synthesis from adenosine diphosphate (ADP)[130]. ROS are naturally generated as a byproduct of the ETC[131,132] particularly when electrons are transferred between complexes I and III[133–135]. Notably, ROS also serve as important cell signaling molecules in coordination with other redox metabolites like GSH. For instance, ROS/GSH redox signaling has been shown to drive activation and commitment in MuSCs[50,136]. In addition to OXPHOS, the TCA cycle takes place within the mitochondria, oxidizing Acetyl-CoA to generate high-energy electron carriers such as NADH and $FADH_2$, some ATP, and a host of intermediate metabolites[137,138] which respectively have their own roles in cell signaling and contribute to other biosynthetic pathways[139–144].

1.7.2 Mitochondrial dynamics

Mitochondrial dynamics refers to the tightly-regulated and constantly-occurring processes of fission and fusion which modify the morphology of mitochondria in order to respond to cell-intrinsic and -extrinsic stimuli[145,146]. Mitochondrial dynamics are key in maintaining the integrity of the mitochondrial network and are directed by a family of dynamin-related large GTPases[147]. Fragmentation or fusion of the two mitochondrial membranes is achieved through the energy from GTP hydrolysis, which allows these enzymes to perform mechanical work on the inner and outer mitochondrial membranes (IMM and OMM, respectively)[145]. Mitochondrial fission and fusion have distinct functions within the cell. For instance, fission segregates damaged components of the mitochondrial network and can target them for removal via autophagy, while fusion enables the functional complementation of these dysfunctional components as well as the distribution of metabolites and mitochondrial proteins throughout the network[148].

Mitochondrial fusion occurs on both the inner and outer mitochondrial membranes, beginning with OMM fusion. OMM fusion is mediated by the dynamin-related GTPase MFN1 (Mitofusin 1)[149]. Through GTP hydrolysis, MFNs undergo a conformational change that enables the contact and fusion of two distinct OMMs[150]. The fusion of the IMM is regulated by OPA1 (Optic atrophy 1), a GTPase with additional roles in cristae architecture and integrity[151–153]. OPA1 exists in long (L-OPA1) and short (S-OPA1) isoforms, however L-OPA1 is membrane-anchored and the only isoform contributing to mitochondrial fusion[154,155]. During IMM fusion, OPA1 interacts with mitochondrial cardiolipin, a phospholipid which stabilizes membrane curvature

during fusion. Like with the OMM, GTP hydrolysis by OPA1 drives conformational changes that allow for the contact and fusion of IMMs[156,157].

Mitochondrial fission occurs first at the OMM and then the IMM. It is initiated following actin polymerization and the contact between endoplasmic reticulum (ER) tubules with the OMM, leading to its constriction[158]. DRP1 (Dynamin-related protein 1) is a GTPase that remains in its inactive form within the cytosol, but can be post-translationally modified to become activated[159,160]. The most well-characterized modification that promotes DRP1 activation is its phosphorylation at the Ser616 residue[159]. Once active, DRP1 becomes translocated to the OMM to physically interact with the adaptors Fis1 (Mitochondrial fission 1), MFF (Mitochondrial fission factor), or MID49/MID51 (Mitochondrial dynamics protein 49 and 51)[145,161]. At the fission site on the OMM, DRP1 oligomerizes into a ring-like complex to constrict the membrane, segmenting mitochondria into two distinct organelles[147,162].

Despite their differing roles, both fission and fusion are critical to mitochondrial homeostasis; the balance of these processes is essential to cellular function. Knock-outs of the fusion modulators MFN1/2 and OPA1 impact cellular health and mitochondrial function, leading to dysregulated metabolism, loss of membrane potential, reduced respiration rates, and reduced cellular growth rates[153,163–165]. Complete knock-outs of DRP1, OPA1, and MFN1/2 have been shown to induce severe mitochondrial dysfunction and are embryonically lethal in mice[149,166–168]. As such, mitochondrial dynamics are essential to cellular health and function.

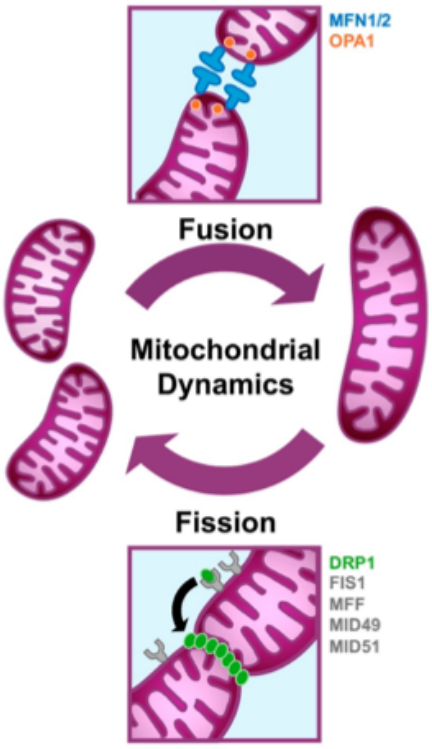

Figure 5. Overview of mitochondrial dynamics. Mitochondrial dynamics is regulated by a family of large GTPases. Mitochondrial morphology undergoes constant, balanced cycles of fission and fusion, which each occur on both the inner and outer mitochondrial membranes. Fusion at the outer mitochondrial membrane is modulated by MFN1/2, and at the inner mitochondrial membrane, OPA1. Fission of both membranes is regulated by the GTPase DRP1 in its active form and its adaptors FIS1, MFF, MID49, and MID51. Figure adapted from Sommers, Tomsine, & Khacho. (2024). *Cells*.

1.7.3 Roles of mitochondrial dynamics in muscle stem cell activity and fate

From quiescence to terminal myogenic differentiation, the mitochondrial network undergoes continual morphological changes, with associated changes in cell signaling and metabolism[113,134,166]. During quiescence, the mitochondrial network has an elongated morphology which influences the depth of their dormancy; a more fragmented network functionally primes MuSCs for activation in a state of G_{alert}[50]. MuSC activation is stimulated through systemic HGF/mTOR signaling, which is required to induce mitochondrial fission[50]. As MuSCs become activated, mitochondrial fission occurs through the downregulation of OPA1 expression[50] and the upregulation of DRP1[169]. Interestingly, in models such as OPA1-KO MuSCs, which exhibit a more fragmented mitochondrial network, there is a significant increase in the mTOR pathway constituent pS6[50], which is also an established marker of the G_{alert} state[42]. Acute loss of OPA1 is also associated with enhanced kinetics of cell cycle entry, while transgenic overexpression of OPA1 in MuSCs conversely shows a more elongated mitochondrial network, a greater depth of

quiescence, and delayed activation kinetics[50]. Notably, the mitochondrial fission that is characteristic of activated MuSCs is associated with a transient physiological increase in mitochondrial ROS in coordination with glutathione (GSH)[50]. Treating MuSCs with rotenone to stimulate ROS generation or with GSH is sufficient to upregulate *MyoD* and *MyoG* gene expression while simultaneously downregulating *Pax7* and *CD34* gene expression[50], suggesting the exit from a quiescent state and an enhanced propensity to commit to myogenic differentiation. When MuSCs undergo the fate decisions of commitment to myogenic differentiation or self-renewal, they can be differentiated by their expression levels of Pax7, whereby committed MuSCs exhibit low Pax7 levels and self-renewing MuSCs are high in Pax7 expression[35,170]. Notably, in other stem cell populations, it has been widely shown that stem cell commitment is promoted by mitochondrial fission[136,171–173]. Consistently, our lab has shown that during the process of self-renewal in MuSCs, elongation of the mitochondrial network is a feature of the return to quiescence[50].

In conclusion, the transient changes in expression of key mitochondrial dynamics regulators like OPA1 are essential for proper MuSC function and activity. Further, these findings demark the essential role for coordinated changes in mitochondrial dynamics in MuSC activity and fate, from quiescence until terminal myogenic differentiation.

1.8 Mitochondrial dysfunction-associated cellular senescence

Mitochondrial dysfunction is a conserved feature associated with senescent and aged-like phenotypes[97,111]. It is simultaneously true that mitochondrial dysfunction maintains cellular senescence[107,174], and senescence contributes to senescence-associated mitochondrial dysfunction (SAMD)[174]. For instance, there is a notable dysregulation of the mitochondrial proteome in MuSCs during aging that is associated with proliferation defects and hallmarks of cellular senescence. Zeng *et al*. showed that the RNA-binding protein responsible for post-translational control of the mitochondrial proteome, CPEB4, becomes down-regulated in different aged tissues, and when depleted in MuSCs, induces cellular senescence[93]. Interestingly, restoring CPEB4 in aged animals rescued defects in the mitochondrial metabolome and improved geriatric MuSC functions[93].

Other forms of mitochondrial dysfunction, such as oxidative stress and excessive ROS accumulation have equally been shown to promote a senescent phenotype, such as through the stimulation of the DNA damage response (DDR). γ-H2AX[64, 166] represents the phosphorylation of

the Ser139 residue of histone variant H2AX[167]. As part of the early cellular response to double-stranded breaks (DSBs) during the DDR, γ-H2AX+ foci accumulate in the nucleus[167]. As such, γ-H2AX+ foci are considered to be a sensitive marker of the DDR and cellular senescence. This mechanism is conserved across many cell types, including MuSCs; MuSCs isolated from aged mouse and human muscle preferentially express the DDR marker γ-H2AX[64, 166].

Through the mitochondrial metabolome, MuSCs dynamically regulate their genome epigenetically throughout the myogenic program[43,175,176]. Of all the states of MuSCs, proliferating MuSCs have the greatest levels of histone acetylation[175]. It is suggested that this is due to the metabolic switch in MuSCs, which have higher Acetyl-CoA levels as they switch from fatty acid oxidation during quiescence[43] to glycolysis in activation[120], and later OXPHOS following differentiation[129]. Comparatively, as cells progress towards differentiation, H3K27 trimethylation marks accumulate, repressing Pax7 gene expression. Cencioni *et al*. describe this marker as being "hoarded" in aged muscle cell chromatin, which was associated with higher levels of senescence-associated heterochromatin foci (SAHFs)[177]. Consistently, they showed that acetylation at the H3K9 residue was significantly reduced, limiting chromatin accessibility[177]. RNAseq showed a downregulation of genes involved in cell cycle progression, differentiation, and DNA repair, and an upregulation of inflammation and senescence-associated genes[177]. While the precise mechanism is not fully known, H3K27 methylation has also been shown to compromise the G_1/S and G_2/M transitions by repressing Cyclin D, CDK4, and CDK6 levels in myoblasts[178]. Relatedly, in geriatric mice, there is epigenetic derepression of the $p16^{Ink4a}$ locus: Sousa-Victor *et al.* suggest that this drives a pre-senescent state which occurs through loss of H2A monoubiquitylation at the K119 residue, a major repressor of this locus[87]. Dysregulated $p16^{Ink4a}$ activation is also shown to induce insufficient production of myoblasts for muscle repair and exhaustion of the MuSC pool[120]. In this way, it is possible that changes in the MuSC metabolome are capable of modifying MuSC cell cycle regulation through changes in the epigenetic landscape.

Inflammation and fibrosis are hallmarks of aging and are associated with the SASP[106]. Interestingly, in retinal epithelial cells, impaired mitochondrial dynamics have been associated with transcriptomic changes that induce inflammatory responses related to the SASP[146]. Importantly, while the SASP can reinforce the senescent state of MuSCs, it can equally stimulate senescence in nearby MuSCs and other cycling cells as well[89]. Additionally, Yu *et al.* investigated the role of PGAM5, a phosphatase of DRP1, in retinal epithelial cell senescence. They found that

PGAM5-KO mutations lead to mitochondrial hyperfusion, reduced mitochondrial turnover, and stimulation of the AMPK-mTOR pathway via ATP and ROS production, leading to premature senescence[146]. PGAM5-KO cells were shown to have elevated levels of γ-H2AX, p16, p53, IL-6, and MMP3, all conserved markers of senescence and the SASP[146,179]. These studies indicate that it is not excessive fragmentation or elongation of the mitochondria alone, but imbalanced mitochondrial dynamics as a whole, which can induce precocious aging or senescent phenotypes. In summary, there are a number of mechanisms in which mitochondrial dysfunction is shown to stimulate senescence in MuSCs and other muscle cells, leading to the impaired generative capacity of skeletal muscle.

Chapter 2: Hypothesis & Aims

2.1 Rationale

Regulators of mitochondrial dynamics experience a decline in expression at both the transcript and protein levels with age in the whole skeletal muscle and the MuSCs of aging mice and humans[50,180,181]. Notably, while MFN1/2 and DRP1 also become dysregulated during aging in the whole muscle, it is only the loss of OPA1 protein that correlates with a decline in muscle quality with age[181]. Tezze *et al*. show in their whole muscle-specific model of chronic OPA1 loss that mice have a precocious aging phenotype, developing white hairs and kyphosis, a reduction in myofiber number, reduced specific force generation, and an upregulation of pro-inflammatory cytokines including IL-6[180]. Not only does chronic loss of OPA1 impair whole muscle quality, but it also induces epithelial senescence in these animals, with significant increases in p21 and β-galactosidase systemically[180]. In sedentary elderly patients, decline of OPA1 expression is correlated with a 38% decline in muscle mass and mitochondrial dysfunction[181].

In our lab's conditional, MuSC-specific OPA1-KO (OPA1-MKO) model, the effects of chronic OPA1 loss were previously described following 1- or 3-months post-tamoxifen administration (post-TAM). Freshly isolated 3-month OPA1-KO myofibers were associated with significantly more Pax7+ MuSCs co-expressing pS6[50], the mTOR pathway constituent and an indicator of the G_{alert} state[42]. Between 0 and 4 hours of culture, 3-month OPA1-KO MuSCs displayed signs of enhanced activation kinetics, indicated by a greater proportion of MuSCs co-expressing Pax7 and MyoD[50]. This finding suggests that chronic OPA1 loss is linked to a disruption in the balance between myogenic differentiation and self-renewal, much like in aged MuSCs. Further, at 7 days following cardiotoxin (CTX) injury, 3-month post-TAM OPA1-MKO muscle experiences regeneration defects and significant Pax7+ cell depletion[50]. This may indicate an exhaustion of the quiescent MuSC pool, possibly through the reduced propensity to self-renew, or through other means, including cellular senescence. Our research group has also previously shown that at 1-month post-TAM, OPA1-KO MuSCs have a lower propensity to express Ki67 following 24 hours of culture, but are capable of passing through the G_1/S cell cycle transition point[50]. In comparison, 3-month post-TAM OPA1-KO MuSCs show a significant reduction in Ki67 levels and undergo complete arrest at the G_1/S transition[50]. Following 72 hours of culture, while 3-month OPA1-WT MuSCs form larger clusters as they proliferate, OPA1-KO clusters are limited to approximately 1 cell on average[50], indicating a remarkable deficit in proliferation. We

now seek to understand whether these cell cycle and proliferative defects can be referred to as cellular senescence.

Chronic imbalances of mitochondrial fission and fusion are a form of mitochondrial dysfunction, and chronic imbalances in mitochondrial dynamics have equally been shown to induce phenotypes of cellular senescence[107,146]. Additionally, the enhanced mitochondrial fragmentation occurring during aging and in pathologies associated with stem cell exhaustion have also been linked to OPA1 deficiencies[182,183]. It has been shown in other cell types that imbalanced mitochondrial dynamics stimulate premature senescent phenotypes, including stimulation of the DDR, upregulation of cell cycle inhibitors, and increased expression of SASP components[146]. While it is well-established that loss of OPA1 occurs naturally with age in MuSCs and whole skeletal muscle and that these deficits contribute to phenotypes of accelerated aging and cellular senescence, the particular role of chronic OPA1 loss in inducing a senescent phenotype in MuSCs is not known.

2.2 Hypothesis

Chronic loss of the mitochondrial fusion protein OPA1 is sufficient to induce a senescent phenotype in muscle stem cells.

2.3 Aims

To investigate the role of chronic OPA1 loss in muscle stem cell maintenance and activity, there are three research aims:

1. Determine if there is a role for OPA1 and mitochondrial dynamics in inducing a senescent phenotype in muscle stem cells.
2. Investigate how mitochondrial dynamics and chronic loss of OPA1 can induce irreversible cell cycle arrest in muscle stem cells.
3. Understand the impacts of chronic OPA1 loss in the context of muscle stem cell maintenance and muscle physiology.

Chapter 3: Materials & Methods

3.1 Mouse model

Pax7CreERT2 mice[175] were crossed with OPA1$^{flox/flox}$ mice[176] (kindly provided by Dr. Ruth Slack) to generate a conditional knock-out of OPA1 in Pax7+ adult MuSCs in a tamoxifen-inducible system (*OPA1-Pax7CreERT2*, referred to as OPA1-MKO). Mice with the OPA1-flox allele that expressed the CreERT2 recombinase were used as OPA1 MuSC knock-out (OPA1-MKO) mice; littermates that were OPA1-floxed but did not express the CreERT2 recombinase were utilized as wild-type controls (OPA1-WT). Tamoxifen administration (200 mg/kg) (Sigma J63509.06) occurred at 8-10 weeks of age via oral gavage for five days. For a model of chronic OPA1 loss, all animals were allowed to age up 4, 12, 26, or 39 weeks (1-9 months) following tamoxifen administration prior to experimentation. Animal protocols were approved by the University of Ottawa Animal Care Ethics Committee and were in accordance with the guidelines of the Canadian Council on Animal Care. Mice were maintained at the University of Ottawa Animal Care and Veterinary Service facility.

3.2 Muscle injury model

30 minutes prior to Cardiotoxin (CTX) injection, mice were subcutaneously injected with Buprenorphine (0.1 mg/kg) and anesthetized by gas inhalation. 50 µL of 10 µM Cardiotoxin (Sigma 217503-1MG) in phosphate buffered saline (PBS) were injected into the *tibialis anterior* (TA) muscle with a 28G-1/2 insulin syringe. The injured muscles were considered to be the muscles injected with CTX; the contralateral limb remained uninjured. Mice subjected to CTX injection recovered in a cage with a heating pad and were monitored 24 hours post-injection. Muscles from the injured limbs were harvested following cervical dislocation at 14 days post-injury (DPI).

3.3 Muscle harvest

Muscle harvest for histology

At the time of isolation, *tibialis anterior* (TA) muscles were harvested following cervical dislocation and immediately transferred to 2% (w/v) PFA (Sigma P6148), on ice. Following 30 minutes of fixation on a rocker, the muscle was washed with cold 1X PBS, then with cold 0.25M glycine twice for 10 minutes. The glycine was decanted, and 5% w/v

sucrose was added for 2 hours, on ice and at 4°C. The TAs were then transferred to an Eppendorf 1.5 mL tube with 20% (w/v) sucrose, rocking at 4°C for 2-3 days. Subsequently, TAs were embedded in Optimal Cutting Temperature (OCT) compound (VWR CA95057-838) and frozen in isopentane for 30 seconds, cooled by liquid nitrogen, and immediately stored at -80°C for long-term storage.

Muscle harvest for gene expression analysis

At the time of isolation, TA muscles were harvested following cervical dislocation, dried on a Kimwipe, and immediately flash-frozen in liquid nitrogen. The frozen tissues were subsequently stored at -80°C for long-term storage until RNA was extracted.

3.4 Isolation of muscle stem cells

At the time of isolation, all hindlimb skeletal muscle tissue was harvested following cervical dislocation then digested in gentleMACS C-Tubes (Miltenyi Biotec 130-093-237) in a solution containing 1% (w/v) Collagenase B (Roche 11088831001) and 0.4% (w/v) Dispase II (Roche 4942078001), then dissociated for 27 minutes using a Miltenyi Gentle-MACS Octo-Dissociator with the SLICE-FACS program. The resulting muscle slurry was filtered with a 100 µm cell strainer (FisherBrand 22363549), divided evenly into two 15 mL tubes, and spun at 600g for 10 minutes. The supernatant was aspirated from each tube, and pellets were resuspended and combined in 400 µL of red blood cell lysis buffer (Sigma R7757) and incubated for 30 seconds. 10 mL of FACS Buffer (3mM EDTA, 10% (v/v) FBS in 1X PBS) were added to the re-combined sample, which was then spun at 600g for 5 minutes. The supernatant was aspirated, then the pellet was resuspended in 1 mL of FACS Buffer. The samples were incubated with PE-conjugated antibodies, including the following Lin- antibodies to negatively select against non-muscle stem cells within the sample: CD31 (2 µL/mouse, BD Pharmigen 553373); CD45 (2 µL/mouse, BD Pharmigen 553081); CD11b (2 µL/mouse, eBioscience 12-0112-82); and Sca1 (2 µL/mouse, BD Pharmigen 553108), as well as VCAM (10 µL/mouse, Biolegend 105720) and α-integrin-7 (10 µL/mouse, Ablab 67-0010-05) to positively select for muscle stem cells within the sample (Table 2). Following incubation, FACS buffer was added to the sample for a final volume of 15 mL and spun at 600g for 5 minutes. The supernatant was aspirated, and the pellet was resuspended in 1 mL of FACS buffer. The sample was then filtered using a 50 µm CellTrics cell filter (Sysmex 04-

004-2327) and brought to the Beckman Coulter MoFlo XDP at the Ottawa Hospital Research Institute's Flow Cytometry and Cell Sorting Facility to be sorted.

3.5 Single myofiber isolation and culture

At the time of isolation, extensor digitorum longus (EDL) muscles were harvested following cervical dislocation and immediately transferred to 2 mL of pre-warmed (37°C) digestion solution (0.5% (w/v) Collagenase B (Roche 11088831001), 1% (v/v) Penicillin-Streptomycin (Wisent Bioproducts 450-201-EL) in DMEM). EDL muscles were incubated in the digestion solution for 35-45 minutes at 37°C to allow single myofibers to be released. Once digested, the EDL muscles were transferred to an FBS-coated 6-well plate containing DMEM with 1% (v/v) Penicillin-Streptomycin. The ends of pipette tips were cut off to be small-bore, then sterilized and coated with FBS. The digested EDLs were triturated using the small-bore FBS-coated pipette tips to enable further release of single myofibers. Single myofibers were washed twice before resting for 10 minutes prior to being transferred to 1 mL of culture media (DMEM 4.5 g/L glucose, 20% (v/v) FBS, 1% (v/v) chicken embryo extract (CEE), 1% (v/v) penicillin-streptomycin), and 7.5 ng/mL bFGF) in a 24-well plate. Culture conditions were at 37°C, 5% CO2 and ranged for 24-48 hours in accordance with the experimental design. Single myofibers remained untreated or were treated with 1 mM L-Glutathione (GSH; Sigma G4251) or 200 µM uridine (Sigma U3750-1G). At the time of collection (T=24 or T=48h), single myofibers were fixed in pre-warmed (37°C) 2% (w/v) PFA for 10 minutes and washed 3x5 minutes with 1X PBS at room temperature. For EdU labelling and detection, myofibers were pulsed with 10µM EdU (BaseClick BCN-001-500) 1 hour before the collection point and labelled with the EdU Cell Proliferation Kit for Imaging (BaseClick BCK-EdU647IM100) according to the manufacturer's instructions prior to staining with primary antibodies.

3.6 Histological analysis

Freshly isolated primary MuSCs

Freshly FACS-isolated MuSCs were collected, accounting for a volume of 200 µL cell suspension (20,000 cells) per slide. Cell suspensions were pipetted into CytoFunnels and centrifuged with the CytoSpin at 1000 rpm for 5 minutes on the 'high' acceleration setting. Slides were removed and cells were immediately fixed in 2% (w/v) PFA for 10 minutes

then washed 3x5 minutes with 1X PBS at room temperature. Cells were permeabilized for 10 minutes with 0.1% Triton X-100 in H_2O then incubated in blocking solution (10% FBS in 1X PBS) for 2 hours at room temperature in a humidified chamber. Primary antibodies diluted in 5% FBS in 1X PBS were added to the samples and incubated overnight at 4°C (see Table 2 for working concentrations). Cells were washed 3x5 minutes before adding secondary antibodies diluted in in 5% FBS in 1X PBS to incubate for 1 hour (see Table 2 for working concentrations). At the end of the incubation, DAPI (diluted 1:1000 in 1X PBS) was added for 5 minutes, then cells were washed, and coverslips were mounted with Immumount (ThermoFisher 9990402). Cytospun MuSCs were visualized at 63X magnification on the Zeiss Axio.Observer Epifluorescent microscope in the Khacho Lab at the University of Ottawa.

Single EDL fibers

Single EDL fibers were incubated in 1 mL of permeabilization solution (0.1% (v/v) Triton-X 100, 0.1 M glycine in 1X PBS) prior to blocking for 5 hours in blocking solution (5% (v/v) horse serum, 2% (w/v) BSA, 0.1% (v/v) Triton-X 100 in 1X PBS) on a rocker at room temperature. Primary antibodies were diluted in blocking solution (see Table 2 for working concentrations) and incubated overnight on a rocker at 4°C. 3x5 minutes washes with 1X PBS were performed. Then, secondary antibodies were diluted in blocking solution (see Table 2 for working concentrations) and incubated for an hour, light-covered, on a rocker at room temperature. Fibers were then mounted using Immumount (ThermoFisher 9990402) on charged glass slides (Fisher Scientific, 12-550-15). MuSCs residing on the single isolated EDL myofibers were visualized at 63X magnification on the Zeiss Axio.Observer Epifluorescent microscope in the Khacho Lab at the University of Ottawa.

Tissue sections

Tissue sectioning

14 µm thick cross-sections of the TA muscle were obtained using the HM425NX Cryostat (University of Ottawa Histology Core) at -28°C and placed on charged glass slides. Three tissue cross-sections were added to each charged slide and were stored at -80°C until further analysis.

Immunofluorescence staining of muscle tissue sections

Antigen retrieval of the tissue sections was performed by the Louise Pelletier Histology Core Facility at the University of Ottawa with citrate buffer (pH=6.0). Around each tissue section on the slide, a circle was drawn with a hydrophobic marker (Thermo Scientific R3777). Sections were washed with 1X PBS for 2 minutes and aspirated with a vacuum system. Sections were blocked in 3% (w/v) BSA (Tocris 5217) for 1 hour at room temperature in a humidified chamber. Primary antibodies (Table 2) diluted in 3% BSA were added overnight at 4°C then subsequently washed 5x2 minutes with 1X PBS. Sections were incubated for 30 minutes with IgG-specific biotin in 3% BSA in the humified chamber and washed for 5x2 minutes with 1X PBS. Sections were then incubated with secondary antibodies and DAPI (Table 2) diluted in 3% BSA for 15 minutes at room temperature and washed again for 5x2 minutes with 1X PBS. The circle of hydrophobic marker was then removed. Coverslips (Fisher Scientific 12541033CA) were mounted with Immumount (Fisher Scientific 9990402). Slides were allowed to dry, light-covered, overnight and subsequently stored at 4°C. Stained sections were imaged on the Zeiss AxioObserver.Z1 Epifluorescent microscope or with the Leica Thunder Epifluorescent microscope, each at 20X magnification with the stitched tile feature at the University of Ottawa's Cell Biology Image Acquisition Core.

Triple fiber type immunofluorescence staining of muscle tissue sections

Slides were retrieved from storage at -80°C. Condensation was removed, and circles were drawn around each section with a hydrophobic marker. Slides air dried for 10 minutes then were washed with 1X PBS. Sections were blocked with 10% (v/v) goat serum in 1X PBS for 1 hour at room temperature then washed 3 times with 1X PBS. Primary antibodies (Table 2) were diluted in 10% goat serum and added to each section for 2 hours at room temperature. Sections were washed for 3x5 minutes with 1X PBS. Secondary antibodies (Table 2) were diluted in 10% goat serum and incubated for 1 hour at room temperature, then subsequently

washed once with PBS. 40X TrueBlack Plus (Biotium 23014) was diluted to a 1X concentration in 1X PBS to quench the sections for 5 minutes. Sections were washed for 3x5 minutes before drying and mounting with coverslips with Immumount. Slides were allowed to dry, light-covered, overnight and subsequently stored at 4°C. Stained sections were imaged on the Leica Thunder Epifluorescent microscope at 10X magnification with the stitched tile feature at the University of Ottawa's Cell Biology Image Acquisition Core. Procedure was performed in accordance with the protocol and using the antibodies generously provided by Menzies Lab at the University of Ottawa.

Hematoxylin & eosin staining of muscle tissue sections

Frozen slides were retrieved from storage at -80°C and stained for hematoxylin and eosin (H&E) by the Louise Pelletier Histology Core Facility at the University of Ottawa. Stained sections were imaged on the EVOS FLAuto2 belonging to the Burelle Lab at the University of Ottawa.

Lipid droplet staining of muscle tissue sections

Frozen slides were retrieved from storage at -80°C and stained for lipid droplets using Oil Red O staining by the Louise Pelletier Histology Core Facility at the University of Ottawa. Slides were imaged on the same day they were prepared with both the EVOS FLAuto2 belonging to the Burelle Lab (with transmitted light) and the Leica Thunder Epifluorescent microscope at the University of Ottawa's Cell Biology Image Acquisition Core.

3.7 Gene expression analysis

RNA isolation from isolated muscle stem cells

The PicoPure RNA column-based isolation kit (ThermoFisher KIT0214) was utilized to isolate total RNA from MuSC pellets in accordance with the manufacturer's instructions. The isolated MuSC RNA was immediately quantified using the NanoDrop 2000 Spectrophotometer, aliquoted, then stored at -80°C until further analysis.

RNA isolation from whole muscle

Muscles were MagNAlysed in 1 mL of Trizol reagent three times in total, with 1-minute incubations between each lysis period. Samples were then incubated at room temperature for 5 minutes. 200 µL of chloroform were then added and incubated at room temperature for 2 minutes. The samples were then centrifuged for 15 minutes at 10000 rpm at 4°C. The upper aqueous phase was collected and 500 µL of isopropanol were added to each sample. Samples were incubated overnight at -80°C, and the next day, were thawed at room temperature and centrifuged for 15 minutes at 10000 rpm at 4°C. The supernatant was aspirated, and the RNA pellet was washed with 75% ethanol and centrifuged for 10 minutes at 10000 rpm at 4°C. The supernatant was aspirated, and the RNA pellet was dried for 10 minutes, inverted over a KimWipe. Dried pellets were resuspended in Gibco distilled water (Fisher 15230162).

Quantitative real-time PCR (RT-qPCR)

RNA was diluted to a concentration of 5 ng/µL and prepared for RT-qPCR using the RotorGene SYBR RT-qPCR kit (Qiagen 204174). All samples were run in triplicates and with a housekeeping gene (GAPDH or B-Actin) for normalization. The following thermal cycler program settings were utilized on the RotorGene Thermalcycler: 55°C for 10 minutes, 95°C for 5 minutes, cycling of 95°C for 5 seconds and 60°C for 10 seconds for 40 repeat cycles, melting from 60-95°C with a 1°C rise each step with 90 seconds of pre-melt conditioning on the first step and 5 seconds for each subsequent step. Each gene was fitted to its respective standard curve and analyzed accordingly.

3.8 Metabolomics of primary muscle stem cells

FACS-isolated cells were centrifuged at 4200 rpm for 2 minutes, and the resulting cell pellet was gently resuspended in 2 mL of ice cold 150 mM ammonium formate buffer in a bead beater tube before gently spinning the cells down. The buffer was removed, and cells were placed on ice before adding 380 µL of 50% (v/v) MeOH in water and 6 sterile ceramic beads, then vortexing. 220 µL of ice cold acetonitrile were added to the samples and vortexed. The samples were then put in a bead beater and beat for 2 minutes at 30 Hz. 600 µL of ice-cold dichloromethane and 300 µL of

ice cold water were added to the samples, vortexed for 1 minute, then allowed to partition on ice for 10 minutes. Samples were then centrifuged for 10 minutes at 4000 rpm at 1°C. The upper aqueous phase was transferred to a new, pre-chilled Eppendorf tube and dried using a chilled speed-vac and stored at -80°C until ready for LC-MS injection and data collection by the University of Ottawa Metabolomics Core. Analysis of significantly differentially regulated metabolites (log fold-change ≥ 2.0, p-value ≤ 0.05) were analyzed using the MetaboAnalyst program.

3.9 Resipher analysis of isolated single myofibers

Resipher experiment

Single myofibers were isolated as described above and washed three times with 1% penicillin-streptomycin in DMEM, careful to remove all debris. 20 myofibers were transferred to each experimental well of the NUNC 96-well plate. Culture media (DMEM 4.5 g/L glucose, 20% (v/v) FBS, 1% (v/v) chicken embryo extract (CEE), 1% (v/v) penicillin-streptomycin), and 7.5 ng/mL bFGF) was added to a final volume of 175 µL. 175 µL of sterile 1X PBS was added to all empty wells. Each sample was plated in triplicates. Fibers were allowed to settle for 10 minutes prior to adding the Resipher Sensing Lid and beginning the experiment. The oxygen flux (i.e., oxygen consumption rate) data was obtained via the Resipher Software and exported at 15-minute intervals.

Normalization

At the endpoint, each well's contents were transferred to individual 1.5 mL tubes and washed twice with 1X PBS at 4200 rpm for 3 minutes. The supernatant was removed, and the tubes containing the myofiber pellets were transferred to liquid nitrogen before storing at -80°C until protein was extracted. For protein extraction of the myofibers, protease inhibitors (Sigma PPC1010) were prepared at a 1:100 dilution in RIPA buffer (Sigma R0278). 15 µL of the cocktail were added to each sample and incubated for 15 minutes. The samples were then centrifuged at 4200 rpm for 3 minutes and the supernatant was collected. A DC Assay was performed to measure the total protein content for each Resipher well's contents, run in triplicates. Each oxygen flux data point was subsequently normalized to total protein content.

3.10 ELISA

Blood was extracted from mice prior to sacrifice via cardiac puncture and immediately collected in EDTA-coated tubes (Sarstedt 41.1395.105). Blood was spun at 2000g for 15 minutes at room temperature. The supernatant (plasma) was transferred to a 1.5 mL tube and stored at -80°C until further analysis. FGF-21 levels in plasma were measured using the ProteinTech Mouse/Rat FGF-21 ELISA Kit (ProteinTech KE10095) and IL-6 levels in plasma were measured using the ProteinTech Mouse IL-6 ELISA Kit (ProteinTech KE10007), each according to manufacturer directions. For the FGF-21 ELISA, 12.5 µL of plasma per duplicate were utilized (1:8 dilution); for the IL-6 ELISA, 25 µL of plasma per duplicate were utilized (1:4 dilution).

3.11 Physiological analysis of whole skeletal muscle

Preparation and dissection

At the time of analysis, mice were injected with 10 µL/g of body mass of 240 mg/mL pentobarbital intraperitoneally in their lower quadrant. The TA muscle was exposed, and fascia was removed to expose the caudal tendon. Thread was passed underneath the tendon and tied to keep the muscle in tension. Electrodes were placed on the exterior side of the quadriceps and maintained parallel to one another. Dissections and preparations were kindly performed by Dr. Junio Dort's Lab at the University of Ottawa. At the end of the experiment, animals were euthanized, and the TA muscle was isolated to measure the length and mass. For the mass, an average of three measurements was used for each sample.

Assessment of contractile properties

In the 610A Dynamic Control Lab Book software, a new study was created in accordance with the animal parameters (sex, strain, mass, age, and genotype) as well as the sample parameters (mass and length of the muscle). For force frequency analysis, the TA muscle was stimulated at 10, 25, 50, 80, 100, 120, and 150 Hz with periods of rest in between each stimulus. The absolute force (mN) was normalized to the length (mm) and mass (mg) to determine the specific force (N/cm^2) of the TA. For fatiguability analysis, the TA muscle was stimulated at 100 Hz, inducing sequential contractions for 2 minutes (60 contractions).

Each value was expressed as a percentage of the force generated at the first contraction (% initial force).

3.12 Statistical analysis

Statistical analyses were performed in Excel (student's paired and un-paired t-tests). All statistics are presented with the following significance: $p < 0.05$ *, $p < 0.01$ **, $p < 0.001$ ***.

Primer	Forward Sequence (5'→3')	Reverse Sequence (5'→3')	Method
OPA1 flox	TTAAGACACCCCAAGAGCTTGC	CCAGCTTAGATCCCATTTGTTGACAG	Genotyping
Control	TTACGTCCATCGTGGACAGC	TGGGCTGGGTGTTAGCCTTA	Genotyping
Cre	GAACCTGATGGACATGTTCAGG	AGTGCGTTCGAACGCTAGAGCCTGT	Genotyping
Atrogin1	GCAAACACTGCCACATTCTCTC	CCTGAGGGGAAAGTGAGACG	RT-qPCR
B-Actin	AAATCGTGCGTGACATCAAA	AAGGAAGGCTGGAAAAGAGC	RT-qPCR
CCND1	GCGTACCCTGACACCAATCTC	CTCCTCTTCGCACTCTGCTC	
CDKN1a (p21)	CCTGGTGATGTCCGACCTG	CCATGAGCGCATCGCAATC	RT-qPCR
CDKN2a (p16)	CGCAGGTTCTTGGTCACTGT	TGTTCACGAAAGCCAGAGCG	RT-qPCR
Cdk4	ATGGCTGCCACTCGATATGAA	TCCTCCATTAGGAACTCTCACAC	RT-qPCR
GAPDH	TCGGTGTGAACGGATTTG	GGTCTCGCTCCTGGAAGA	RT-qPCR
Murf1	GTGTGAGGTGCCTACTTGCTC	GCTCAGTCTTCTGTCCTTGGA	RT-qPCR

Table 1. Sequences of primers used for genotyping and RT-qPCR.

Method	Antibody	Company / Catalog Number	Dilution	Antibody Type
FACS	PE rat anti-mouse CD31	BD Pharmingen 553373	2 µL/animal	Negative selection
	PE rat anti-mouse CD45	BD Pharmingen 553081	2 µL/animal	Negative selection
	PE rat anti-mouse CD11b	eBiosciences 12-0112-82	2 µL/animal	Negative selection
	PE rat anti-mouse Sca1	BD Pharmingen 553108	2 µL/animal	Negative selection
	PE-Cy7 conjugated CD106 (VCAM)	Biolegend 105720	10 µL/animal	Positive selection
	647 conjugated alpha integrin 7 (rat)	Ablab 67-0010-05	10 µL/animal	Positive selection
Immunofluorescent Staining of MuSCs	Pax7 (mouse)	DHSB PAX7-S	1:13	Primary
	Pax7 (rabbit)	Invitrogen PA1-117	1:50	Primary
	CD47 (mouse)	BD Biosciences 555297	1:200	Primary
	γ-H2AX (rabbit)	Cell Signaling Technology 2577S	1:250	Primary
	Ki67 (rabbit)	Abcam AB-15580	1:1000	Primary
	pRb (rabbit)			Primary
	Cy3 (mouse)	Jackson 715-165-150	1:1000	Secondary
	Cy3 (rabbit)	Jackson 711-165-152	1:1000	Secondary
	Alexa-Fluoro 488 (mouse)	Invitrogen A11001	1:1000	Secondary
	Alexa-Fluoro 488 (rabbit)	Invitrogen A11008	1:1000	Secondary

Immunofluorescent Muscle Fiber Type Staining of Tissue Sections	BA-F8 Mouse IgG_{2b} (MHCI)	DHSB	1:50	Primary
	SC-71 Mouse IgG1 (MHCIIa)	DHSB	1:50	Primary
	BF-F3 Mouse IgM (MHCIIb)	DHSB	1:50	Primary
	Anti-laminin alpha 2 Rat IgG1(4H8-2)	Santacruz SC-59854	1:50	Primary
	Alexa Fluor Plus 405 Anti-Rat IgG	Invitrogen A48261	1:500	Secondary
	Alexa Fluor 488 Anti-Mouse IgM	Invitrogen A21042	1:500	Secondary
	Alexa Fluor 594 Anti-Mouse IgG_{2b}	Invitrogen A21145	1:500	Secondary
	Alexa Fluor 647 Alpaca Anti-Mouse IgG1	ChromoTek CTK0103	1:500	Secondary
Immunofluorescent Staining of Tissue Sections	Pax7 (mouse)	DHSB PAX7-S	1:13	Primary
	MyoD (mouse)	Santa Cruz SC-32758	1:100	Primary
	Ki67 (rabbit)	Abcam 15580	1:1000	Primary
	Laminin (rabbit)	Abcam 11575	1:1000	Primary
	eMHC (mouse)	DHSB F1.652-S	1:15	Primary
	Alexa-Fluor 488 (rabbit)	Invitrogen A11008	1:500	Secondary
	Alexa-Fluor 647 (mouse)	Invitrogen AB-150107	1:500	Secondary
	Biotin	Jackson Immuno 115-065-205	1:250	Secondary
	Streptavidin-Cy3	Jackson Immuno 016-160-084	1:250	Secondary

Table 2. Antibodies used for immunofluorescent (IF) staining or fluorescence-activated cell sorting (FACS) and their working dilutions.

Chapter 4: Results

4.1 The duration of OPA1 loss in muscle stem cells is associated with a progressive accumulation of senescence markers and dysregulation of cell cycle genes

Our lab has previously shown that chronic loss of OPA1 leads to enhanced activation kinetics, proliferative defects, and mitochondrial dysfunction in MuSCs, therefore mimicking an aged-like phenotype[50]. To assess whether chronic loss of OPA1 in MuSCs is sufficient to induce a senescent phenotype, OPA1-KO MuSCs were freshly isolated at 1- or 3-months post-tamoxifen administration (post-TAM) via fluorescence-activated cell sorting (FACS) to identify whether markers of cellular senescence accumulate with chronic OPA1 loss, as compared to aged-matched OPA1-WT controls. We utilized immunofluorescence to determine whether at 1- or 3-months post-TAM, OPA1-KO MuSCs accumulate γ-H2AX+ foci in the nucleus or CD47 at the cell surface (Figure 6A, 6D). While at 3-months post-TAM there was significant difference in fluorescence intensity for either marker between the OPA1-KO and OPA1-WT (Figure 6B, 6E), the OPA1-KO MuSCs have a greater number of γ-H2AX+ foci (Figure 6F), indicative of a stimulation of the DDR and a conserved marker of cellular senescence across many cell types[146,184,185]. Further, a greater proportion of MuSCs exhibit a preferential localization of CD47 at their cell surface in the OPA1-KO relative to the OPA1-WT at 3-months post-TAM (Figure 6C), an established marker of senescent MuSCs in particular[89]. Similarly, at 1-month post-TAM, a greater proportion of OPA1-KO MuSCs accumulate CD47 at the cell surface relative to the OPA1-WT (Figure 6I), though there is no significant difference in the number of γ-H2AX+ foci at this time (Figure 6K). Thus, with increased duration of OPA1 ablation, MuSCs accumulate hallmarks of cellular senescence.

Given that our lab previously described proliferative defects in chronic OPA1-KO MuSCs[50] and that these cells show evidence of cellular senescence, we next sought to characterize their transcriptional regulation of the G_1/S cell cycle phase via RT-qPCR. In freshly FACS-isolated OPA1-KO MuSCs, the gene expression of the positive cell cycle modulators Cyclin D (*CCND1*) and CDK4 (*Cdk4*) and negative cell cycle modulators p16 (*CDKN2A*) and p21 (*CDKN1A*) were analyzed at 1- and 3-months post-TAM relative to age-matched wild-type controls. At 1-month post-TAM, OPA1-KO MuSCs have a significant reduction in Cyclin D relative to the OPA1-WT (Figure 7A). By 3-months post-TAM, Cyclin D expression is not restored and remains significantly downregulated relative to the OPA1-WT (Figure 7E). Additionally, there is an

upregulation in p21 expression in the 3-month OPA1-KO MuSCs (Figure 7G). These findings are consistent with the G_1/S defects our lab has previously described, where at 3-months post-TAM, OPA1-KO MuSCs fail to meaningfully express Ki67 (the proliferative marker) and pRb (indicating passage through the R-point) in culture[50]. Consistently, it is also known that during senescence, Rb hypophosphorylation can occur through the inhibition of CDK4-Cyclin D, such as by p21, which ultimately blocks cell entry into the S-phase of the cell cycle[186]. Despite an upregulation of p21 expression at 3-months post-TAM (Figure 7G), there was no significant difference in the other cell cycle inhibitor and marker of senescence, p16, in the OPA1-KO compared to the OPA1-WT (Figure 7F).

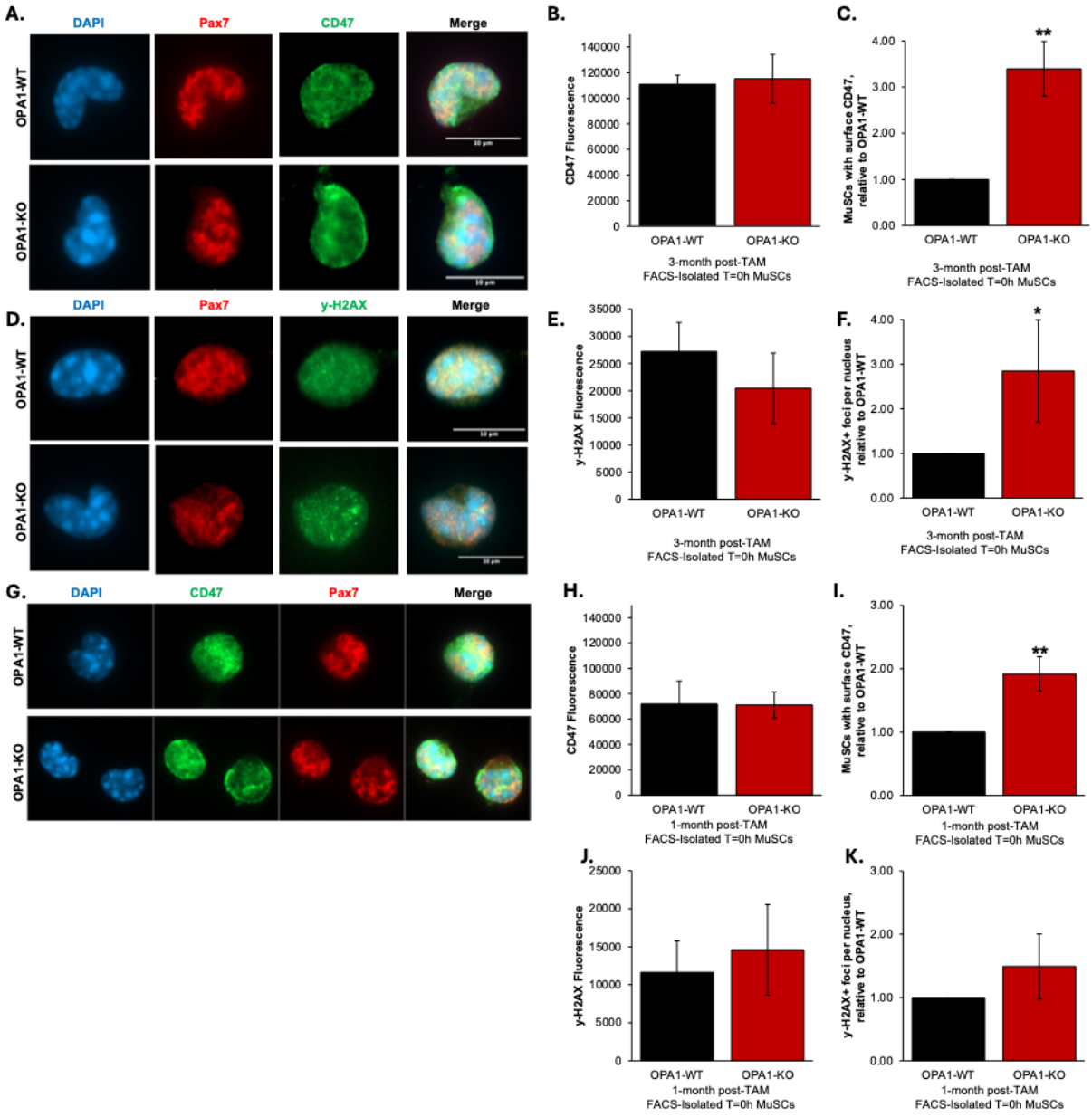

Figure 6. Chronic loss of OPA1 is associated with an accumulation of senescence markers in muscle stem cells. **A.** Representative image of CD47 localization in 3-months post-TAM T=0h OPA1-WT and OPA1-KO MuSCs. **B.** CD47 fluorescence intensity in 3-months post-TAM T=0h OPA1-WT and OPA1-KO MuSCs (N=3 independent experiments, ± SD, n.s.). **C.** Proportion of MuSCs with CD47 localizing at the cell surface, relative to OPA1-WT in 3-months post-TAM MuSCs (N=3 independent experiments, ± SD, p=0.0022). **D.** Representative image of γ-H2AX foci in 3-months post-TAM T=0h OPA1-WT and OPA1-KO MuSCs. **E.** γ-H2AX fluorescence intensity in 3-months post-TAM T=0h OPA1-WT and OPA1-KO MuSCs (N=3 independent experiments, ± SD, n.s.). **F.** Number of γ-H2AX foci per nucleus, relative to OPA1-WT in 3-months post-TAM MuSCs (N=3 independent experiments, ± SD, p=0.0490). **G.** Representative image of CD47 localization in 1-month post-TAM T=0h OPA1-WT and OPA1-KO MuSCs. **H.** CD47 fluorescence intensity in 1-month post-TAM T=0h OPA1-WT and OPA1-KO MuSCs (N=3 independent experiments, ± SD, n.s.). **I.** Proportion of MuSCs with CD47 localizing at the cell surface, relative to OPA1-WT in 1-month post-TAM MuSCs (N=3 independent experiments, ± SD, p=0.0042). **J.** γ-H2AX fluorescence intensity in 1-month post-TAM T=0h OPA1-WT and OPA1-KO MuSCs (N=3 independent experiments, ± SD, n.s.). **K.** Number of γ-H2AX foci per nucleus, relative to OPA1-WT in 1-month post-TAM MuSCs (N=3 independent experiments, ± SD, n.s.).

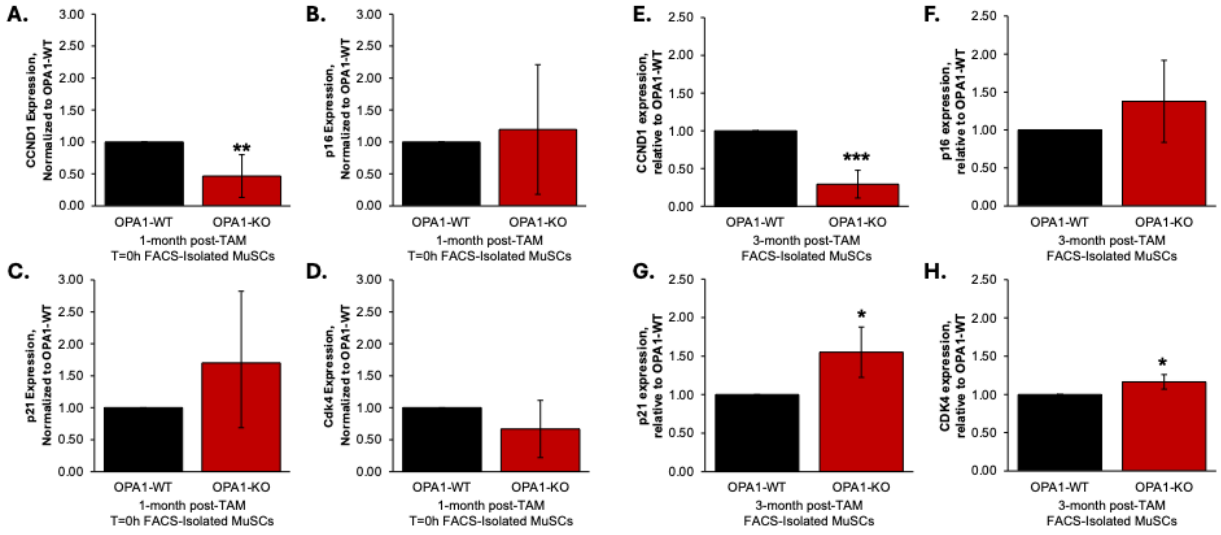

Figure 7. Chronic loss of OPA1 in muscle stem cells leads to cell cycle defects at the transcriptional level. (A-D). Gene expression of cell cycle modulator genes in 1-month post-TAM T=0h OPA1-WT and OPA1-KO MuSCs, quantified via RT-qPCR, normalized to GAPDH expression and relative to OPA1-WT (N=3 independent experiments, ± SD): **A.** *CCND1* (p=0.0026) ; **B.** p16 (*CDKN1A,* n.s.); **C.** p21 (*CKDN2A*, n.s.*)*; **D.** Cdk4 (n.s.). **(E-H).** Gene expression of cell cycle modulator genes in 3-months post-TAM T=0h OPA1-WT and OPA1-KO MuSCs, quantified via RT-qPCR, normalized to GAPDH expression and relative to OPA1-WT (N=3 independent experiments, ± SD): **E.** *CCND1* (p=0.0026) ; **F.** p16 (*CDKN1A,* n.s.); **G.** p21 (*CKDN2A*, p=0.0431); **H.** Cdk4 (p=0.0402).

4.2 Chronic loss of OPA1 is associated with global changes in the muscle stem cell metabolome.

We next sought to characterize the global alterations in the metabolome associated with chronic OPA1 loss in MuSCs. In this way, we aimed to gain insight on possible sources of metabolic dysregulation which may explain the stem cell dysfunction in 3-month OPA1-KO MuSCs. To do so, we performed LC-MS/MS metabolomics on 3-month post-TAM OPA1-WT and OPA1-KO MuSCs. From this, we identified 24 significantly differentially regulated metabolites (Figure 8A). Interestingly, of this set, there was only one metabolite, uridine-5-triphosphate (UTP), that was downregulated in the OPA1-KO, while all others were upregulated relative to the OPA1-WT (Figure 8A). Additionally, many of the upregulated metabolites in the OPA1-KO are amino acids and their derivatives, including threonine, aspartic acid, methionine, glutamine, N-acetylalanine, tryptophan, alanine, tyrosine, valine, and leucine (Figure 8A). Pathway enrichment analysis showed an enrichment for glutathione-associated pathways, including cysteine, serine, and glutamate metabolism, as well as pathways involved in nucleotide metabolism and aerobic energy (Figure 8B).

Given that the proliferative defects become more severe with prolonged loss of OPA1 in chronic OPA1-KO MuSCs, we sought to determine whether these defects could be mitigated prior to the onset of complete cell cycle arrest through the supplementation of exogenous metabolites. Our lab has shown that in coordination with ROS, GSH is a key promoter of activation and proliferation in MuSCs, but becomes depleted in 3-months post-TAM OPA1-KO MuSCs[50]. Additionally, uridine is a precursor for UTP which becomes depleted at 3-months post-TAM in OPA1-KO MuSCs (Figure 8A). As our lab has established that uridine stimulates MuSC proliferation (Wade *et al*., in preparation) in addition to GSH, we aimed to improve the proliferative capacity of chronic OPA1-KO MuSCs prior to the initiation of full cell cycle arrest by treating with these metabolites at 1-month post-TAM. Our *in vitro* model involves the isolation and culture of single extensor digitorum longus (EDL) myofibers on which MuSCs reside. 1-month post-TAM OPA1-KO MuSCs from single isolated EDL myofibers were treated with GSH or uridine for T=24 or T=48 hours to analyze the MuSC cell cycle progression relative to the untreated and to OPA1-WT controls. At 24 hours, there was no significant difference in the proportion of Ki67+/Pax7+ or pRb+/Pax7+ MuSCs for either treatment (Figure 8C-8D, 8G-8H). However, supplementation of exogenous GSH and uridine respectively improved the proportion of Ki67+/Pax7+ and EdU+/Pax7+ MuSCs by T=48 hours relative to the untreated condition (Figure 8E-8F, 8I-8J).

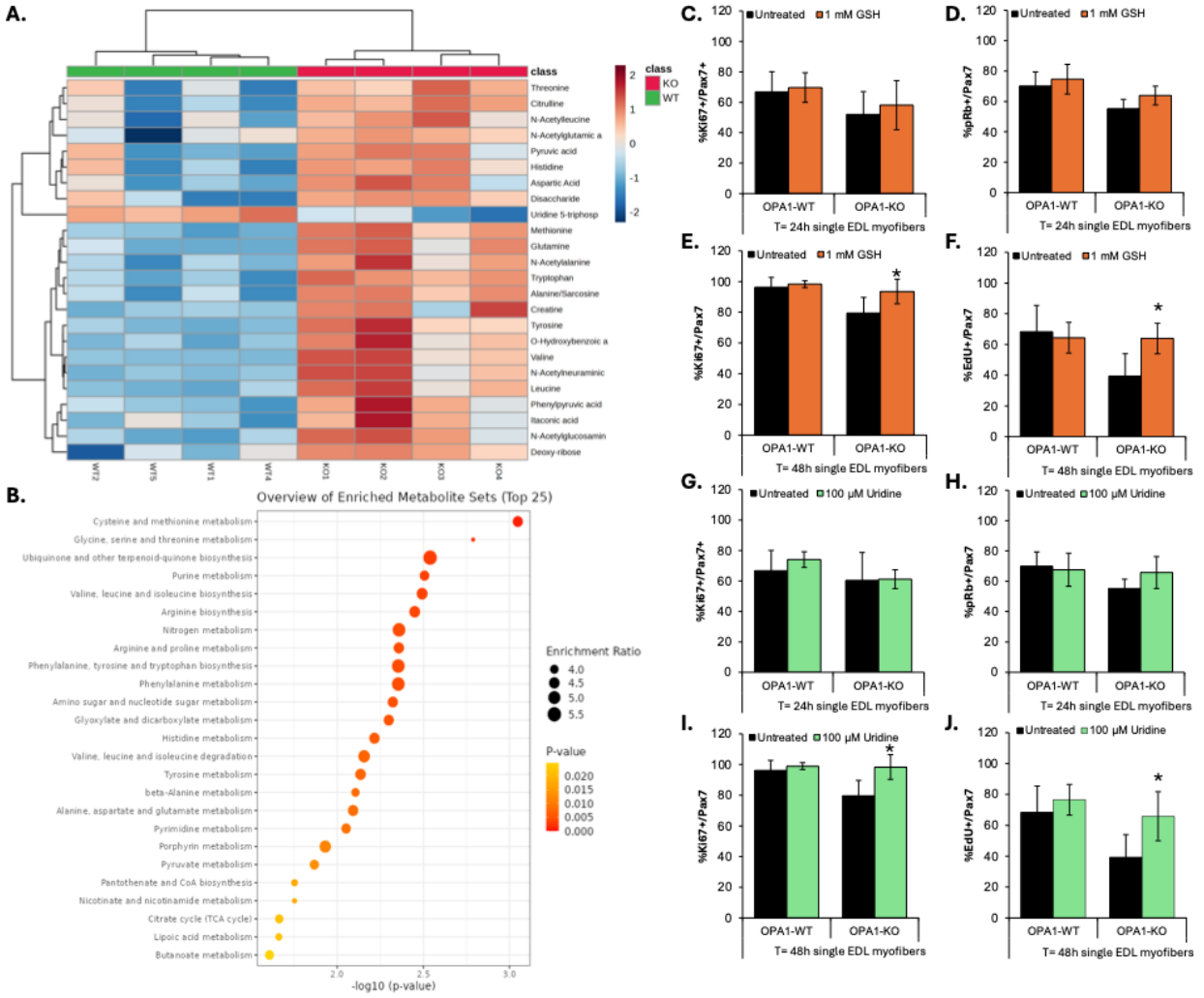

Figure 8. Chronic loss of OPA1 is associated with global changes in the muscle stem cell metabolome. A. Heatmap of the top 25 significantly differentially regulated metabolites in 3-month post-TAM OPA1-KO MuSCs (N=4 biological replicates). **B.** MetaboAnalyst pathway enrichment analysis in 3-month post-TAM OPA1-KO MuSCs (N=4 biological replicates). **C.** Percentage of 1-month post-TAM Pax7+ cells expressing Ki67 at T=24-hours in culture following treatment with 1 mM GSH (N=5 biological replicates, ± SD, n.s.). **D.** Percentage of 1-month post-TAM Pax7+ cells expressing pRb at T=24-hours in culture following treatment with 1 mM GSH (N= 5 biological replicates, ± SD, n.s.). **E.** Percentage of 1-month post-TAM Pax7+ cells expressing Ki67 at T=48-hours in culture following treatment with 1 mM GSH (N= 4 biological replicates, ± SD, p=0.0141). **F.** Percentage of 1-month post-TAM Pax7+ cells expressing EdU at T=48-hours in culture following treatment with 1 mM GSH (N= 4 biological replicates, ± SD, p=0.0032). **G.** Percentage of 1-month post-TAM Pax7+ cells expressing Ki67 at T=24-hours in culture following treatment with 100 µM uridine (N= 5 biological replicates, ± SD, n.s.). **H.** Percentage of 1-month post-TAM Pax7+ cells expressing pRb at T=24-hours in culture following treatment with 100 µM uridine (N= 5 biological replicates, ± SD, n.s.). **I.** Percentage of 1-month post-TAM Pax7+ cells expressing Ki67 at T=48-hours in culture following treatment with 100 µM uridine (N= 4 biological replicates, ± SD, p=0.0024). **J.** Percentage of 1-month post-TAM Pax7+ cells expressing EdU at T=48-hours in culture following treatment with 100 µM uridine (N= 4 biological replicates, ± SD, p=0.0377).

4.3 Chronic loss of OPA1 in muscle stem cells causes significant regeneration deficits and stem cell depletion following injury.

To evaluate whether disruption of mitochondrial dynamics in MuSCs impairs the regenerative capacity of skeletal muscle, we implemented an *in vivo* injury model and compared the phenotype in injured OPA1-WT and OPA1-MKO TA muscles at 14 days post-injury (DPI). At 1-month post-TAM, OPA1-MKO muscle exhibited significant regenerative defects, with a significant reduction in the myofiber cross-sectional area (CSA) and in centrally nucleated (regenerating) myofibers (Figure 9B, 9C). Newly formed myofibers transiently express eMHC, which as the myofibers mature, gets downregulated while adult isoforms of MHC increase in abundance. Notably, by 14 DPI, 1-month post-TAM OPA1-MKO muscle shows a significant increase in the proportion of eMHC+ myofibers relative to the OPA1-WT, suggesting the onset of myofiber formation but a failure to become mature myofibers by this timepoint (Figure 9E). To assess whether chronic loss of OPA1 affected MuSC fate decisions *in vivo* in this model, we quantified the proportion of Pax7+ and MyoD+ cells per 1000 μm^2, and in both instances, found a significant reduction in the 1-month post-TAM OPA1-MKO relative to the OPA1-WT (Figure 9G, 9J). When quantifying the proportion of these cell populations that co-expressed the proliferative marker Ki67, we did not observe any significant difference between the two genotypes (Figure 9H, 9K).

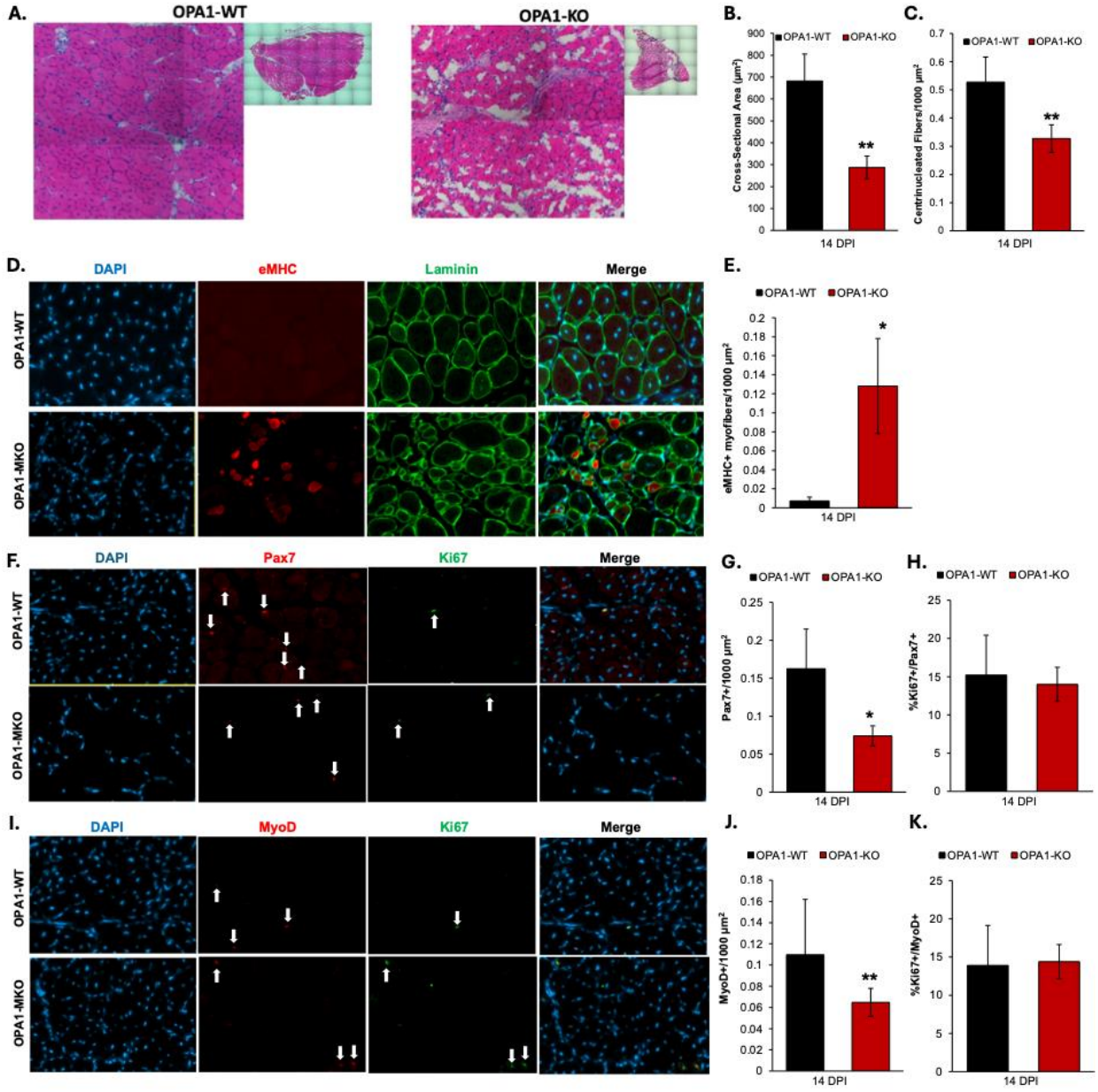

Figure 9. Chronic loss of OPA1 in muscle stem cells causes significant muscle regeneration defects. Cardiotoxin injury experiment in 1-month post-TAM OPA1-WT and OPA1-MKO TA muscles at 14 days-post injury (DPI) **A.** Representative image of H&E-stained OPA1-WT and OPA1-MKO muscle at 14 DPI. Visualized at 20X magnification on the EVOS FLAuto2. **B.** Cross-sectional area (μm^2) of OPA1-WT and OPA1-MKO myofibers at 14 DPI (N=4 biological replicates; ± SD , p=0.0033). **C.** Centrinucleated myofibers per 1000 μm^2 in OPA1-WT and OPA1-MKO TAs at 14 DPI (N=4 biological replicates; ± SD, p=0.0019). **D.** Representative image of eMHC+ myofiber distribution in OPA1-WT and OPA1-MKO TAs at 14 DPI. Visualized at 20X on the Zeiss.Z1 Epifluorescent microscope. White arrows indicate towards positive cells. **E.** eMHC+ myofibers per 1000 μm^2 in OPA1-WT and OPA1-MKO TAs at 14 DPI (N=4 biological replicates; ± SD, p=0.0190). **F.** Representative image of Pax7+ and Ki67+ cell distribution in OPA1-WT and OPA1-MKO TAs at 14 DPI. Visualized at 20X on the Zeiss.Z1 Epifluorescent microscope. White arrows indicate towards positive cells. **G.** Number of Pax7+ cells per 1000 μm^2 in OPA1-WT and OPA1-MKO TAs at 14 DPI (N=4 biological replicates; ± SD , p=0.0467). **H.** Proportion of Ki67+/Pax7+ cells in OPA1-WT and OPA1-MKO TAs at 14 DPI (N=4 biological replicates; ± SD , n.s.). **I.** Representative image of MyoD+ and Ki67+ cell distribution in OPA1-WT and OPA1-MKO TAs at 14 DPI.

Visualized at 20X on the Zeiss.Z1 Epifluorescent microscope. White arrows indicate towards positive cells. **J.** Number of MyoD7+ cells per 1000 μm^2 in OPA1-WT and OPA1-MKO TAs at 14 DPI (N=4 biological replicates; ± SD , p=0.0014). **K.** Proportion of Ki67+/MyoD+ cells in OPA1-WT and OPA1-MKO TAs at 14 DPI (N=4 biological replicates; ± SD, n.s.).

4.4 Chronic loss of OPA1 leads to basal stem cell depletion, the onset of a muscle wasting program, and fatiguability defects within the skeletal muscle.

Our lab has previously shown that at 3-months post-TAM, OPA1-KO MuSCs exhibit cell cycle defects, reduced cluster sizes in culture, and defective regeneration following CTX injury[50]. We therefore asked whether more drastic effects could be observed at increased durations of OPA1 loss, at 6- or 9-months post-TAM. We firstly aimed to characterize the MuSC population basally within the TA muscles of OPA1-WT and OPA1-MKO animals at these time points. Immunofluorescent staining of 6-month and 9-month post-TAM OPA1-MKO TAs for the MuSC marker Pax7 revealed that in the absence of a strong activation stimulus such as injury, there is a significant reduction in the MuSC population basally (Figure 10A, 10G). Interestingly, while the defect is present at 6-months post-TAM, the MuSC population is further depleted by 9-months post-TAM. This finding was reproduced *in vitro* in freshly isolated MuSCs from single EDL myofibers, with significantly fewer Pax7+ cells per myofiber in the OPA1-KO at 6- and 9-month post-TAM relative to the OPA1-WT (Figure 10, 10H).

With this significant defect in the MuSC population, we asked whether there were also defects in the whole muscle that could be identified histologically in the OPA1-MKO at 6- and 9-months post-TAM. At 6-months post-TAM, there was no evidence of atrophy, with no significant difference in the CSA of myofibers or the total number of myofibers per 1000 μm^2 (Figure 10B, 10C). Interestingly, by 9-months post-TAM, OPA1-MKO TA muscles basally show a reduction in the mean myofiber CSA and a reduction in the number of myonuclei per myofiber (Figure 10I, 10J). Due to the presence of this muscle-wasting phenotype at 9-months post-TAM, we asked whether there was any significant difference in atrogene expression in OPA1-WT and OPA1-MKO TA muscles to suggest the onset of the atrophy program at a transcriptional level. When quantifying the expression of the atrogenes *Atrogin1* and *Murf1*, we found no significant difference between the OPA1-WT and OPA1-MKO (Figure 10N, 10O). There was also no significant difference in the presence of FGF-21 (an indicator of fibrosis) or IL-6 (a pro-inflammatory cytokine) in the plasma of OPA1-WT and OPA1-MKO animals at 9-months post-TAM (Figure 10P, 10Q).

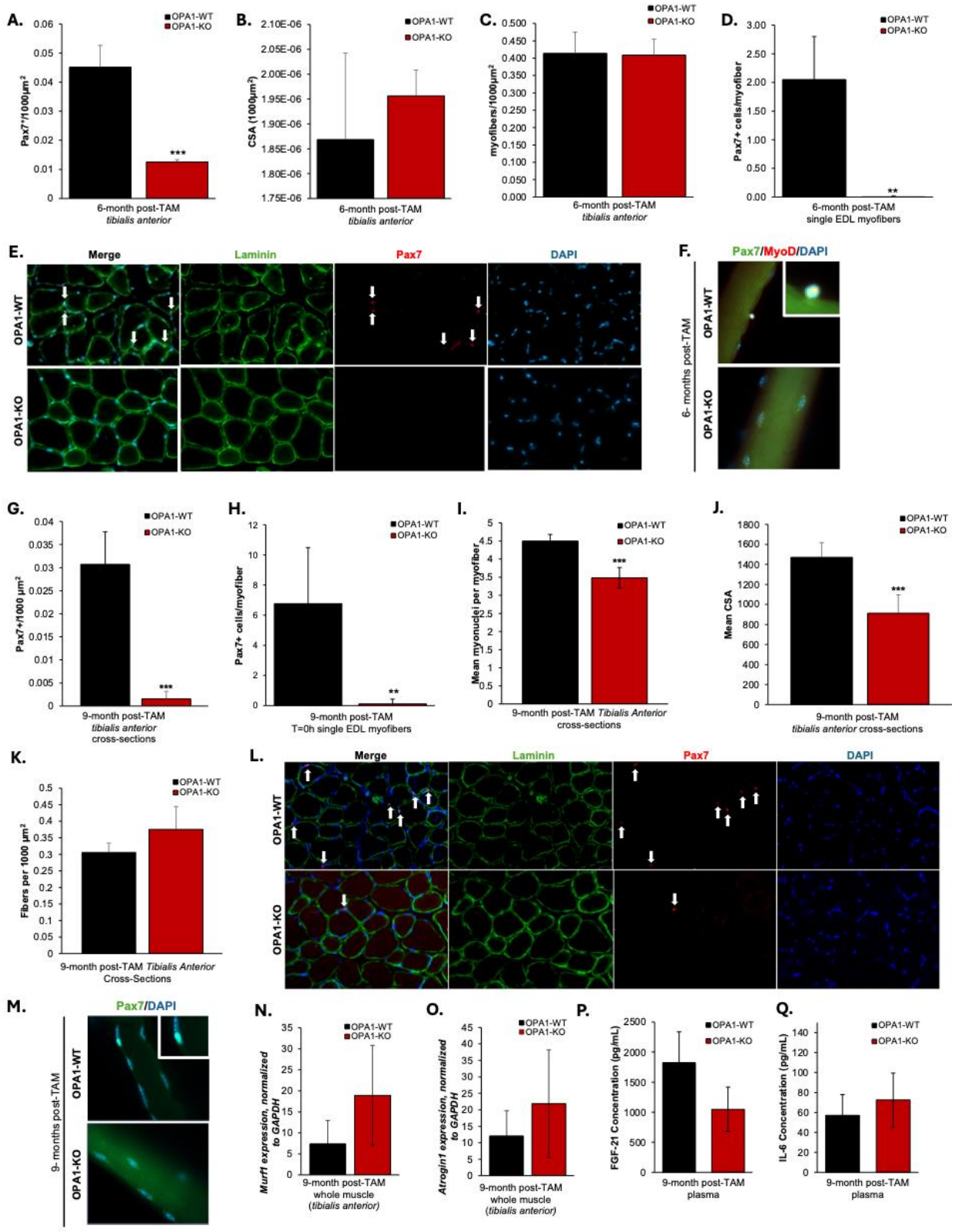

Figure 10. Chronic loss of OPA1 in muscle stem cells is associated with basal stem cell depletion and the onset of a muscle wasting phenotype. A. Number of Pax7+ cells per 1000 µm^2 in 6-months post-TAM OPA1-WT and OPA1-MKO uninjured *tibialis anterior* (TA) muscles (N=6 biological replicates, ± SD, p=0.0002). **B.** Cross-sectional

area (CSA) of myofibers, in 1000 μm^2, of 6-months post-TAM OPA1-WT and OPA1-MKO uninjured TA muscles (N=6 biological replicates, ± SD, n.s.). **C.** Number of myofibers per 1000 μm^2 in 6-months post-TAM OPA1-WT and OPA1-MKO uninjured *tibialis anterior* (TA) muscles (N=6 biological replicates, ± SD, n.s.). **D.** Number of Pax7+ cells per EDL myofiber at 6-months post-TAM (N=5 biological replicates, ± SD). **E.** Representative image of Pax7+ cell abundance in 6-months post-TAM OPA1-WT and OPA1-KO TA muscle cross-sections. White arrows indicate towards Pax7+ cells. **F.** Representative image of MuSC abundance on 6-months post-TAM OPA1-WT and OPA1-KO single isolated EDL myofibers at T=0h. **G.** Number of Pax7+ cells per 1000 μm^2 in 9-months post-TAM OPA1-WT and OPA1-MKO uninjured TA muscles (N=4 biological replicates, ± SD, p=0.00004). **H.** Number of Pax7+ cells per EDL myofiber at 9-months post-TAM (N=4 biological replicates, ± SD, p=0.0049). **I.** Number of myonuclei per myofiber in 9-months post-TAM OPA1-WT and OPA1-MKO uninjured TA muscles (N=4 biological replicates, ± SD, p=0.0004). **J.** Cross-sectional area (CSA) of myofibers of 9-months post-TAM OPA1-WT and OPA1-MKO uninjured TA muscles (N=4 biological replicates, ± SD, p=0.0017). **K.** Number of myofibers per 1000 μm^2 in 9-months post-TAM OPA1-WT and OPA1-MKO uninjured *tibialis anterior* (TA) muscles (N=4 biological replicates, ± SD, n.s.). **L.** Representative image of Pax7+ cell abundance in 9-months post-TAM OPA1-WT and OPA1-KO TA muscle cross-sections. White arrows indicate towards Pax7+ cells. **M.** Representative image of Pax7+ cell abundance on 9-months post-TAM OPA1-WT and OPA1-KO single isolated EDL myofibers at T=0h. **N.** Gene expression of *Murf1* in whole TA muscles from 9-months post-TAM OPA1-WT and OPA1-MKO animals, quantified by RT-qPCR and normalized to GAPDH expression (N=3 biological replicates, ± SD, n.s.). **O.** Gene expression of *Atrogin1* in whole TA muscles from 9-months post-TAM OPA1-WT and OPA1-MKO animals, quantified by RT-qPCR and normalized to GAPDH expression (N=3 biological replicates, ± SD, n.s.). **(P-Q)** Levels of **P.** FGF-21 and **Q.** IL-6 in the plasma of OPA1-WT and OPA1-MKO mice at 9-months post-TAM (N=6 OPA1-WT, N=8 OPA1-MKO biological replicates, n.s.).

With the reduction in myofiber area, we asked whether there were any associated functional deficits in the whole muscle at 9-months post-TAM in the OPA1-MKO relative to age-matched OPA1-WT controls. Force frequency analysis suggested no significant difference in specific force (N/cm^2) generation with increasing stimulation frequency (Figure 11A), however when assessing for fatiguability, we found that 9-month OPA1-MKO muscle shows a drastic reduction in force generation with sequential stimulation (Figure 11B). This led us to ask whether there were any metabolic changes or defects in the whole muscle that is associated with chronic OPA1 loss in the MuSCs that may explain this fatiguability defect. Through Oil Red O (ORO) histological staining in 9-month post-TAM TAs, we found there was no significant difference in lipid droplet accumulation in the OPA1-WT and OPA1-MKO muscle (Figure 11D). We additionally characterized the fiber type distribution at 9-months post-TAM to possibly explain this defect, however the distribution of MHC type I, IIa, IIb, and IIx myofibers were comparable in the OPA1-WT and OPA1-MKO TA muscles (Figure 11G). We also asked whether there were any differences in the OCR in OPA1-MKO muscle at 3-months post-TAM, potentially due to the stem cell dysfunction observed at this time. We implemented the Resipher platform which utilizes a real-time, live-cell *in vitro* monitoring system to quantify the OCR of single isolated myofibers from 3-month post-TAM OPA1-WT and OPA1-MKO muscle, however there was no significant difference throughout a 24-hour culture period (Figure 11C, 11D).

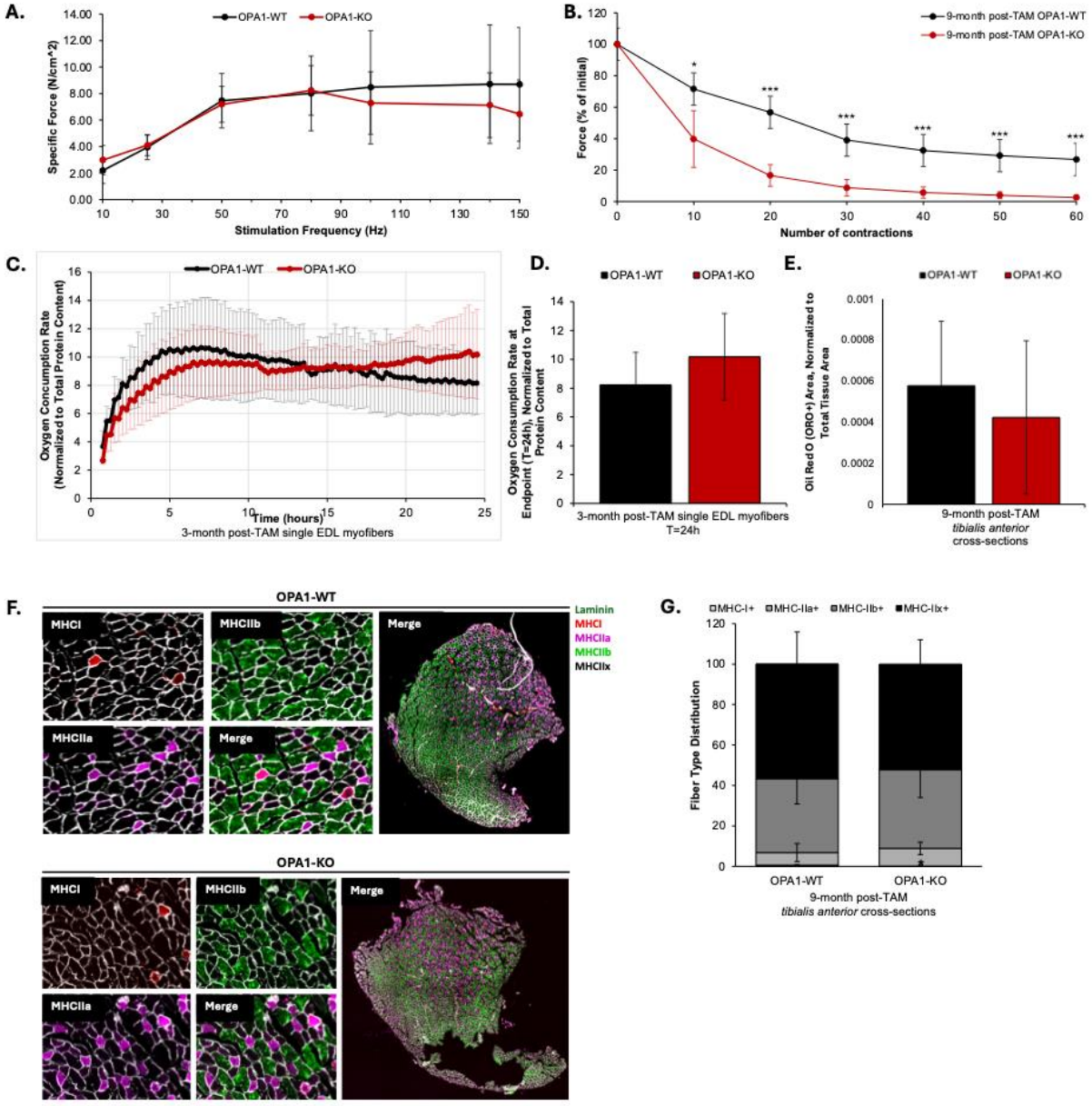

Figure 11. Chronic loss of OPA1 in muscle stem cells leads to functional deficits within skeletal muscle. A. Specific force (N/cm^2) of TA muscle per stimulation frequency in 9-months post-TAM OPA1-WT and OPA1-MKO animals (N=3 biological replicates, ± SD, n.s.). **B.** Force generated by 9-month post-TAM TA muscles per number of sequential contractions expressed as % of initial force in OPA1-WT and OPA1-MKO animals (N=3 biological replicates, ± SD, $p<0.05$*; $p\leq0.0001$***). **C.** Oxygen consumption rate of single EDL myofibers across T=24 hours in culture from 3-months post-TAM OPA1-WT and OPA1-MKO animals, normalized to total protein content (N=3 biological replicates, ± SD, n.s.). **D.** Oxygen consumption rate at endpoint collection (T=24h) of 3-month post-TAM OPA1-WT and OPA1-MKO EDL myofibers, normalized to total protein content (N=3 biological replicates, ± SD, n.s.). **E.** Quantification of Oil Red O+ (ORO+) area in 9-months post-TAM OPA1-WT and OPA1-MKO TA cross-sections, normalized to total tissue area (N=5 biological replicates, ± SD, n.s.). **F.** Representative image of myofiber type distribution at 9-months post-TAM in OPA—WT and OPA1-MKO TA muscle cross-sections. **G.** Myofiber type (MHC type I, IIa, IIb, or IIx) distribution within the TA muscle of OPA1-WT and OPA1-MKO muscle at 9-months post-TAM (N=5 biological replicates, ± SD, MHC-I+: p=0.0386.; MHC-IIa, MHC-IIb, MHC-IIx+: n.s.)

Chapter 5: Discussion

In this work, we investigated the role of chronic OPA1 loss in muscle stem cell maintenance and activity, particularly in an aging context. While our research group previously showed that chronic loss of OPA1 leads to an aged-like phenotype in MuSCs[50], here we show that at 1- and 3-months post-TAM, OPA1-KO MuSCs accumulate markers of cellular senescence. One of the most highly conserved markers of senescence across cell and tissue types is γ-H2AX[184,185,187,188], a replacement histone which becomes phosphorylated early in the repair process of DNA DSBs[185]. CD47 is another marker of cellular senescence, and through alternative polyadenylation, accumulates at the cell surface of senescent MuSCs[89]. Notably, 3-month OPA1-KO MuSCs show a greater number of γ-H2AX+ foci and have a greater propensity to express high levels of CD47 at the cell surface (Figure 6C, 6E). Chronic loss of OPA1 also leads to the downregulation of Cyclin D and the upregulation of p21 expression at 1- and 3-months post-TAM (Figure 7A, 7E), supporting the notion that mitochondrial dysfunction can influence nuclear gene expression to impair the cell cycle progression of MuSCs. Thus, there is evidence supporting the connection between long-term ablation of OPA1 in MuSCs and cellular senescence.

Through our metabolomics analysis, we observed an upregulation of several metabolites in 3-month OPA1-KO MuSCs relative to age-matched OPA1-WT controls, and a significant downregulation in UTP (Figure 8A). In a variety of cell types, cellular senescence is associated with changes in metabolic regulation, including the release of metabolites in response to oxidative stress[189–192]. Senescent cells remain metabolically active and release metabolites, among other factors, through the SASP. It is possible that 3-month OPA1-KO MuSCs, like senescent myoblasts, have a unique exometabolome[112], and that through the release of metabolites, these MuSCs may effect cell signaling functions. However, whether these upregulated metabolites at 3-months post-TAM are accumulating due to enhanced biosynthesis or from disuse remains to be known. At 3-months post-TAM, we observed the accumulation of many amino acids in OPA1-KO MuSCs (Figure 8A). Notably, the accumulation of amino acids is a feature of the unfolded protein response (UPR), when protein synthesis is attenuated to reduce the burden on the ER[193–195]. ER stress is a component of the senescent phenotype[196,197], and phenotypes of mitochondrial dysfunction and dysregulation of the proteome have previously been described in senescent MuSCs[93]. Additionally, loss of OPA1 in the whole skeletal muscle has been shown by Tezze *et al*. to cause ER stress, stimulating the UPR and inducing muscle atrophy and a precocious aging phenotype

systemically[180]. It is therefore possible that a similar mechanism occurs at the stem cell level in 3-month post-TAM OPA1-KO MuSCs to contribute to the senescent phenotype. Due to the depletion of GSH[50] and UTP (Figure 8A) at 3-months post-TAM in OPA1-KO MuSCs, we asked whether we could supplement these metabolites exogenously to mitigate the proliferative defects in OPA1-KO at 1-month post-TAM, prior to the onset of complete G_1/S arrest. We found that 48-hour treatment with exogenous GSH and uridine partially restored the cell cycle progression of OPA1-KO MuSCs at 1-month post-TAM (Figure 8E-8F, 8I-8J). It is therefore possible that within this model of progressive cell cycle dysregulation associated with the duration of OPA1 loss, cell cycle progression can be improved prior to irreversible cell cycle arrest. This knowledge is of interest for the development of preventative measures for disorders associated with the age-related loss of essential mitochondrial dynamics regulators, such as DRP1, MFN1/2, and OPA1[180,181].

Through this work, we also discovered that chronic imbalances in mitochondrial dynamics leads to stem cell depletion basally at 6- and 9-months post-TAM in OPA1-MKO animals (Figure 10A, 10G). Further, at 9-months post-TAM in OPA1-MKO muscle, there is evidence of muscle wasting, with a reduction in the myofiber cross-sectional area and a reduction in the number of myonuclei per myofiber relative to the OPA1-WT (Figure 10I, 10J). Strikingly, when there are chronic imbalances of mitochondrial dynamics within MuSCs, whole muscle defects in fatiguability are observed (Figure 11B). In sum, chronic loss of OPA1 in MuSCs causes an aged-like phenotype in whole skeletal muscle. A popular discussion in the field of regenerative medicine debates the relative contribution of MuSCs to the pathology of muscle atrophy or sarcopenia. The findings from this research present new evidence to this debate and suggest that the presence of dysfunctional MuSCs, such as OPA1-KO MuSCs at 9-months post-TAM, may contribute to the sarcopenic phenotype. Understanding the mechanism by which this occurs will be an important discovery that could inform the development of novel therapeutics for the age-related loss of muscle mass and function, compromising the quality of life in elderly individuals.

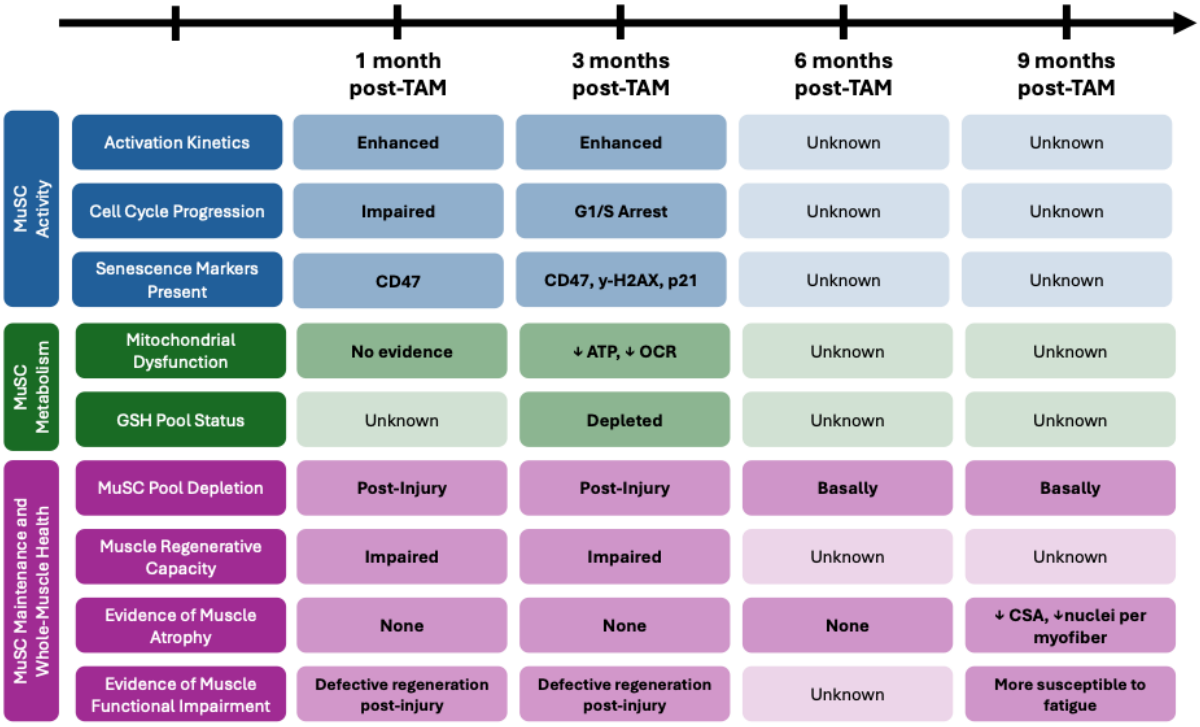

Figure 12. Influences of chronic OPA1 loss on muscle stem cell maintenance and activity, and whole-muscle quality. Phenotypic timeline describing the changes in muscle stem cell (MuSC) activity, metabolism, and maintenance, and whole-muscle health from 1- to 9-months post-TAM in OPA1-MKO animals.

Chapter 6: Conclusion

In conclusion, mitochondrial dynamics is an essential regulator of muscle stem cell activity and fate. Through this research, we have particularly highlighted the importance of OPA1 and mitochondrial dynamics for the proliferative capacity of MuSCs and their maintenance in an aging context. Chronic imbalances in mitochondrial dynamics lead to the accumulation of senescence markers and dysregulation of the G_1/S phase of the cell cycle in MuSCs. However, supplementation of exogenous metabolites can improve the proliferative capacity of MuSCs prior to the onset of complete cell cycle arrest. We have also shown that the presence of dysfunctional MuSCs within the skeletal muscle may contribute to age-associated muscle wasting and fatiguability. Ultimately, our model of chronic OPA1 loss in MuSCs cements the notion that mitochondrial dysfunction, such as through chronic imbalances in mitochondrial dynamics, promotes the onset of senescent and aged-like phenotypes. The findings from this research are of therapeutic interest for sarcopenia and other degenerative diseases associated with impaired mitochondrial dynamics and offer insight on the role of mitochondrial dynamics in inducing MuSC senescence, which has not been described to date.

Chapter 7: Limitations

One limitation of this study is that the process of isolating primary MuSCs inherently serves as an activation stimulus[198,199]. Thus, the process of isolating primary MuSCs via FACS or single EDL myofiber isolation may influence the transcription of cell cycle modulators during the process of activation. To account for this, age-matched wild-type controls are consistently implemented in our research, allowing us to appreciate the differences between the genotypes despite the possibility of influencing cell cycle regulation. Despite this limitation, we have still been able to identify significant defects in cell cycle activity via RT-qPCR in the OPA1-KO relative to the OPA1-WT. Techniques such as *in situ* fixation via perfusion to fix tissues prior to the isolation process may be implemented to bypass this issue by preserving the state in which MuSCs reside in basally, in the absence of an activation stimulus.

A second limitation of this research is that at 9-months post-TAM in the OPA1-MKO muscle, we could not account for the possibility that the dysfunctional OPA1-KO MuSCs may undergo pathological fusion or dysfunctional myonuclear accretion. It is possible that at 9-months post-TAM, if OPA1-KO MuSCs fuse with the myofibers, they could stimulate loss of OPA1 in the whole muscle. As such, it is possible that the fatiguability defects could be associated with the resulting loss of OPA1 in whole skeletal muscle. However, if this pathological fusion does occur, it may be therapeutically relevant and provide insight on how MuSC dysfunction contributes to overall muscle health, like in models of muscular dystrophy.

Chapter 8: Future Directions

While the findings of this research establish a connection between chronic imbalances in mitochondrial dynamics and a senescent phenotype in MuSCs, it would be of great interest to identify the mechanism by which this occurs. For instance, understanding how modulators of mitochondrial dynamics like OPA1 decline in expression with age in MuSCs, or how changes in mitochondrial morphology and metabolism induce cell cycle arrest would be foundational knowledge that could inform therapeutics for degenerative conditions like sarcopenia. Relatedly, identifying the relative contributions of OPA1 in isolation, rather than mitochondrial dynamics as a whole, would be of interest. Beyond its roles in IMM fusion, OPA1 is involved in cristae ultrastructure and supercomplex assembly[151–153], which may distinguish its role in contributing to a senescent phenotype from the other modulators of mitochondrial dynamics. Visualizing mitochondrial ultrastructure and cristae integrity via transmission electron microscopy or studying genetic models which knock-out or overexpress the mitochondrial dynamics regulators MFN1/2 or DRP1 are some ways in which this question could be explored.

Another question that could be explored through future research is the relative contribution of dysfunctional MuSCs to an aged-like or sarcopenic phenotype in whole skeletal muscle. In our model of chronic OPA1 loss at 9-months post-TAM, while the OPA1-KO MuSCs mimic an aged-like phenotype, the animals themselves are only approximately 12 months old. A future approach could be to determine whether the defects that are intrinsic to the MuSCs can be analyzed and understood separately from an aged or dysfunctional local environment, and whether it is the dysfunctional MuSCs alone that are causing the onset of muscle wasting and muscle fatiguability. One way that these questions could be dissected is to perform an engraftment experiment with young, healthy donor MuSCs into the muscle of 9-month post-TAM OPA1-MKO recipient animals and determining whether (1) the young MuSCs can successfully be introduced to the muscle, (2) whether these MuSCs also become depleted or otherwise dysfunctional, and (3) whether introduction of healthy MuSCs can improve the phenotype.

Chapter 9: References

(1) Frontera, W. R.; Ochala, J. Skeletal Muscle: A Brief Review of Structure and Function. *Calcif Tissue Int* **2015**, *96* (3), 183–195. https://doi.org/10.1007/s00223-014-9915-y.

(2) Argilés, J. M.; Campos, N.; Lopez-Pedrosa, J. M.; Rueda, R.; Rodriguez-Mañas, L. Skeletal Muscle Regulates Metabolism via Interorgan Crosstalk: Roles in Health and Disease. *Journal of the American Medical Directors Association* **2016**, *17* (9), 789–796. https://doi.org/10.1016/j.jamda.2016.04.019.

(3) DeFronzo, R. A.; Tripathy, D. Skeletal Muscle Insulin Resistance Is the Primary Defect in Type 2 Diabetes. *Diabetes Care* **2009**, *32* (Suppl 2), S157–S163. https://doi.org/10.2337/dc09-S302.

(4) Guridi, M.; Kupr, B.; Romanino, K.; Lin, S.; Falcetta, D.; Tintignac, L.; Rüegg, M. A. Alterations to mTORC1 Signaling in the Skeletal Muscle Differentially Affect Whole-Body Metabolism. *Skeletal Muscle* **2016**, *6* (1), 13. https://doi.org/10.1186/s13395-016-0084-8.

(5) Wang, Y. X.; Dumont, N. A.; Rudnicki, M. A. Muscle Stem Cells at a Glance. *Journal of Cell Science* **2014**, *127* (21), 4543–4548. https://doi.org/10.1242/jcs.151209.

(6) Dumont, N. A.; Wang, Y. X.; Rudnicki, M. A. Intrinsic and Extrinsic Mechanisms Regulating Satellite Cell Function. *Development* **2015**, *142* (9), 1572–1581. https://doi.org/10.1242/dev.114223.

(7) Schmidt, M.; Schüler, S. C.; Hüttner, S. S.; von Eyss, B.; von Maltzahn, J. Adult Stem Cells at Work: Regenerating Skeletal Muscle. *Cell. Mol. Life Sci.* **2019**, *76* (13), 2559–2570. https://doi.org/10.1007/s00018-019-03093-6.

(8) Ajayi, P. T.; Katti, P.; Zhang, Y.; Willingham, T. B.; Sun, Y.; Bleck, C. K. E.; Glancy, B. Regulation of the Evolutionarily Conserved Muscle Myofibrillar Matrix by Cell Type Dependent and Independent Mechanisms. *Nat Commun* **2022**, *13* (1), 2661. https://doi.org/10.1038/s41467-022-30401-9.

(9) Willingham, T. B.; Kim, Y.; Lindberg, E.; Bleck, C. K. E.; Glancy, B. The Unified Myofibrillar Matrix for Force Generation in Muscle. *Nat Commun* **2020**, *11* (1), 3722. https://doi.org/10.1038/s41467-020-17579-6.

(10) Street, S. F. Lateral Transmission of Tension in Frog Myofibers: A Myofibrillar Network and Transverse Cytoskeletal Connections Are Possible Transmitters. *Journal of Cellular Physiology* **1983**, *114* (3), 346–364. https://doi.org/10.1002/jcp.1041140314.

(11) Goldspink, G. Changes in Striated Muscle Fibres during Contraction and Growth with Particular Reference to Myofibril Splitting. *Journal of Cell Science* **1971**, *9* (1), 123–137. https://doi.org/10.1242/jcs.9.1.123.

(12) Katti, P.; Hall, A. S.; Parry, H. A.; Ajayi, P. T.; Kim, Y.; Willingham, T. B.; Bleck, C. K. E.; Wen, H.; Glancy, B. Mitochondrial Network Configuration Influences Sarcomere and Myosin Filament Structure in Striated Muscles. *Nat Commun* **2022**, *13* (1), 6058. https://doi.org/10.1038/s41467-022-33678-y.

(13) Hynes, T. R.; Block, S. M.; White, B. T.; Spudich, J. A. Movement of Myosin Fragments in Vitro: Domains Involved in Force Production. *Cell* **1987**, *48* (6), 953–963. https://doi.org/10.1016/0092-8674(87)90704-5.

(14) Huxley, A. F.; Niedergerke, D. R. Interference Microscopy of Living Muscle Fibres. **1954**.

(15) Huxley, H.; Hanson, J. Changes in the Cross-Striations of Muscle during Contraction and Stretch and Their Structural Interpretation. *Nature* **1954**, *173* (4412), 973–976. https://doi.org/10.1038/173973a0.

(16) Goody, R. S. The Missing Link in the Muscle Cross-Bridge Cycle. *Nat Struct Mol Biol* **2003**, *10* (10), 773–775. https://doi.org/10.1038/nsb1003-773.
(17) Squire, J. M. Muscle Contraction: Sliding Filament History, Sarcomere Dynamics and the Two Huxleys. *Glob Cardiol Sci Pract 2016* (2), e201611. https://doi.org/10.21542/gcsp.2016.11.
(18) Gomes, A. V.; Potter, J. D.; Szczesna-Cordary, D. The Role of Troponins in Muscle Contraction. *IUBMB Life* **2002**, *54* (6), 323–333. https://doi.org/10.1080/15216540216037.
(19) Littlefield, R.; Almenar-Queralt, A.; Fowler, V. M. Actin Dynamics at Pointed Ends Regulates Thin Filament Length in Striated Muscle. *Nat Cell Biol* **2001**, *3* (6), 544–551. https://doi.org/10.1038/35078517.
(20) Moreland, Z. G.; Jiang, F.; Aguilar, C.; Barzik, M.; Gong, R.; Behnammanesh, G.; Park, J.; Shams, A.; Faaborg-Andersen, C.; Werth, J. C.; Harley, R.; Sutton, D. C.; Heidings, J. B.; Cole, S. M.; Parker, A.; Morse, S.; Wilson, E.; Takagi, Y.; Sellers, J. R.; Brown, S. D. M.; Friedman, T. B.; Alushin, G. M.; Bowl, M. R.; Bird, J. E. Myosin-Based Nucleation of Actin Filaments Contributes to Stereocilia Development Critical for Hearing. *Nat Commun* **2025**, *16* (1), 947. https://doi.org/10.1038/s41467-025-55898-8.
(21) El-Saleh, S. C.; Warber, K. D.; Potter, J. D. The Role of Tropomyosin-Troponin in the Regulation of Skeletal Muscle Contraction. *J Muscle Res Cell Motil* **1986**, *7* (5), 387–404. https://doi.org/10.1007/BF01753582.
(22) Joe, A. W. B.; Yi, L.; Natarajan, A.; Le Grand, F.; So, L.; Wang, J.; Rudnicki, M. A.; Rossi, F. M. V. Muscle Injury Activates Resident Fibro/Adipogenic Progenitors That Facilitate Myogenesis. *Nat Cell Biol* **2010**, *12* (2), 153–163. https://doi.org/10.1038/ncb2015.
(23) Bentzinger, C. F.; Wang, Y. X.; Dumont, N. A.; Rudnicki, M. A. Cellular Dynamics in the Muscle Satellite Cell Niche. *EMBO reports* **2013**, *14* (12), 1062–1072. https://doi.org/10.1038/embor.2013.182.
(24) Abou-Khalil, R.; Mounier, R.; Chazaud, B. Regulation of Myogenic Stem Cell Behaviour by Vessel Cells: The "Ménage à Trois" of Satellite Cells, Periendothelial Cells and Endothelial Cells. *Cell Cycle* **2010**, *9* (5), 892–896. https://doi.org/10.4161/cc.9.5.10851.
(25) Giordani, L.; He, G. J.; Negroni, E.; Sakai, H.; Law, J. Y. C.; Siu, M. M.; Wan, R.; Corneau, A.; Tajbakhsh, S.; Cheung, T. H.; Le Grand, F. High-Dimensional Single-Cell Cartography Reveals Novel Skeletal Muscle-Resident Cell Populations. *Molecular Cell* **2019**, *74* (3), 609-621.e6. https://doi.org/10.1016/j.molcel.2019.02.026.
(26) Relaix, F.; Bencze, M.; Borok, M. J.; Der Vartanian, A.; Gattazzo, F.; Mademtzoglou, D.; Perez-Diaz, S.; Prola, A.; Reyes-Fernandez, P. C.; Rotini, A.; Taglietti. Perspectives on Skeletal Muscle Stem Cells. *Nat Commun* **2021**, *12* (1), 692. https://doi.org/10.1038/s41467-020-20760-6.
(27) Rubenstein, A. B.; Smith, G. R.; Raue, U.; Begue, G.; Minchev, K.; Ruf-Zamojski, F.; Nair, V. D.; Wang, X.; Zhou, L.; Zaslavsky, E.; Trappe, T. A.; Trappe, S.; Sealfon, S. C. Single-Cell Transcriptional Profiles in Human Skeletal Muscle. *Sci Rep* **2020**, *10* (1), 229. https://doi.org/10.1038/s41598-019-57110-6.
(28) Oprescu, S. N.; Yue, F.; Qiu, J.; Brito, L. F.; Kuang, S. Temporal Dynamics and Heterogeneity of Cell Populations during Skeletal Muscle Regeneration. *iScience* **2020**, *23* (4), 100993. https://doi.org/10.1016/j.isci.2020.100993.
(29) Bouche, A.; Borner, B.; Richard, C.; Grand, Y.; Hannouche, D.; Laumonier, T. In Vitro-Generated Human Muscle Reserve Cells Are Heterogeneous for Pax7 with Distinct

Molecular States and Metabolic Profiles. *Stem Cell Research & Therapy* **2023**, *14* (1), 243. https://doi.org/10.1186/s13287-023-03483-5.
(30) *Building Muscle: Molecular Regulation of Myogenesis - PMC*. https://pmc.ncbi.nlm.nih.gov/articles/PMC3281568/ (accessed 2025-02-21).
(31) Cosgrove, B. D.; Gilbert, P. M.; Porpiglia, E.; Mourkioti, F.; Lee, S. P.; Corbel, S. Y.; Llewellyn, M. E.; Delp, S. L.; Blau, H. M. Rejuvenation of the Aged Muscle Stem Cell Population Restores Strength to Injured Aged Muscles. *Nat Med* **2014**, *20* (3), 255–264. https://doi.org/10.1038/nm.3464.
(32) Sambasivan, R.; Yao, R.; Kissenpfennig, A.; Van Wittenberghe, L.; Paldi, A.; Gayraud-Morel, B.; Guenou, H.; Malissen, B.; Tajbakhsh, S.; Galy, A. Pax7-Expressing Satellite Cells Are Indispensable for Adult Skeletal Muscle Regeneration. *Development* **2011**, *138* (17), 3647–3656. https://doi.org/10.1242/dev.067587.
(33) Kuang, S.; Kuroda, K.; Le Grand, F.; Rudnicki, M. A. Asymmetric Self-Renewal and Commitment of Satellite Stem Cells in Muscle. *Cell* **2007**, *129* (5), 999–1010. https://doi.org/10.1016/j.cell.2007.03.044.
(34) Kuang, S.; Gillespie, M. A.; Rudnicki, M. A. Niche Regulation of Muscle Satellite Cell Self-Renewal and Differentiation. *Cell Stem Cell* **2008**, *2* (1), 22–31. https://doi.org/10.1016/j.stem.2007.12.012.
(35) Lepper, C.; Partridge, T. A.; Fan, C.-M. An Absolute Requirement for Pax7-Positive Satellite Cells in Acute Injury-Induced Skeletal Muscle Regeneration. *Development* **2011**, *138* (17), 3639–3646. https://doi.org/10.1242/dev.067595.
(36) Li, L.; Clevers, H. Coexistence of Quiescent and Active Adult Stem Cells in Mammals. *Science* **2010**, *327* (5965), 542–545. https://doi.org/10.1126/science.1180794.
(37) Cheung, T. H.; Rando, T. A. Molecular Regulation of Stem Cell Quiescence. *Nat Rev Mol Cell Biol* **2013**, *14* (6), 329–340. https://doi.org/10.1038/nrm3591.
(38) Rayagiri, S. S.; Ranaldi, D.; Raven, A.; Mohamad Azhar, N. I. F.; Lefebvre, O.; Zammit, P. S.; Borycki, A.-G. Basal Lamina Remodeling at the Skeletal Muscle Stem Cell Niche Mediates Stem Cell Self-Renewal. *Nat Commun* **2018**, *9* (1), 1075. https://doi.org/10.1038/s41467-018-03425-3.
(39) Cheung, T. H.; Quach, N. L.; Charville, G. W.; Liu, L.; Park, L.; Edalati, A.; Yoo, B.; Hoang, P.; Rando, T. A. Maintenance of Muscle Stem-Cell Quiescence by microRNA-489. *Nature* **2012**, *482* (7386), 524–528. https://doi.org/10.1038/nature10834.
(40) *Prepubertal skeletal muscle growth requires Pax7-expressing satellite cell-derived myonuclear contribution | Development | The Company of Biologists*. https://journals.biologists.com/dev/article/145/20/dev167197/48546/Prepubertal-skeletal-muscle-growth-requires-Pax7 (accessed 2025-02-20).
(41) Arjona, M.; Goshayeshi, A.; Rodriguez-Mateo, C.; Brett, J. O.; Both, P.; Ishak, H.; Rando, T. A. Tubastatin A Maintains Adult Skeletal Muscle Stem Cells in a Quiescent State Ex Vivo and Improves Their Engraftment Ability in Vivo. *Stem Cell Reports* **2022**, *17* (1), 82–95. https://doi.org/10.1016/j.stemcr.2021.11.012.
(42) Rodgers, J. T.; King, K. Y.; Brett, J. O.; Cromie, M. J.; Charville, G. W.; Maguire, K. K.; Brunson, C.; Mastey, N.; Liu, L.; Tsai, C.-R.; Goodell, M. A.; Rando, T. A. mTORC1 Controls the Adaptive Transition of Quiescent Stem Cells from G0 to GAlert. *Nature* **2014**, *510* (7505), 393–396. https://doi.org/10.1038/nature13255.
(43) Ryall, J. G.; Dell'Orso, S.; Derfoul, A.; Juan, A.; Zare, H.; Feng, X.; Clermont, D.; Koulnis, M.; Gutierrez-Cruz, G.; Fulco, M.; Sartorelli, V. The NAD+-Dependent SIRT1 Deacetylase

Translates a Metabolic Switch into Regulatory Epigenetics in Skeletal Muscle Stem Cells. *Cell Stem Cell* **2015**, *16* (2), 171–183. https://doi.org/10.1016/j.stem.2014.12.004.
(44) Fu, X.; Xiao, J.; Wei, Y.; Li, S.; Liu, Y.; Yin, J.; Sun, K.; Sun, H.; Wang, H.; Zhang, Z.; Zhang, B.-T.; Sheng, C.; Wang, H.; Hu, P. Combination of Inflammation-Related Cytokines Promotes Long-Term Muscle Stem Cell Expansion. *Cell Res* **2015**, *25* (6), 655–673. https://doi.org/10.1038/cr.2015.58.
(45) Fukada, S.; Ma, Y.; Ohtani, T.; Watanabe, Y.; Murakami, S.; Yamaguchi, M. Isolation, Characterization, and Molecular Regulation of Muscle Stem Cells. *Front. Physiol.* **2013**, *4*. https://doi.org/10.3389/fphys.2013.00317.
(46) Goel, A. J.; Rieder, M.-K.; Arnold, H.-H.; Radice, G. L.; Krauss, R. S. Niche Cadherins Control the Quiescence-to-Activation Transition in Muscle Stem Cells. *Cell Reports* **2017**, *21* (8), 2236–2250. https://doi.org/10.1016/j.celrep.2017.10.102.
(47) Machado, L.; Lima, J. E. de; Fabre, O.; Proux, C.; Legendre, R.; Szegedi, A.; Varet, H.; Ingerslev, L. R.; Barrès, R.; Relaix, F.; Mourikis, P. In Situ Fixation Redefines Quiescence and Early Activation of Skeletal Muscle Stem Cells. *Cell Reports* **2017**, *21* (7), 1982–1993. https://doi.org/10.1016/j.celrep.2017.10.080.
(48) Machado, A. da C.; Barbosa, T. C.; Kluser Sales, A. R.; de Souza, M. N.; da Nóbrega, A. C. L.; Silva, B. M. Adults with Initial Metabolic Syndrome Have Altered Muscle Deoxygenation during Incremental Exercise. *Obesity* **2017**, *25* (2), 424–431. https://doi.org/10.1002/oby.21744.
(49) Velthoven, C. T. J. van; Morree, A. de; Egner, I. M.; Brett, J. O.; Rando, T. A. Transcriptional Profiling of Quiescent Muscle Stem Cells In Vivo. *Cell Reports* **2017**, *21* (7), 1994–2004. https://doi.org/10.1016/j.celrep.2017.10.037.
(50) Baker, N.; Wade, S.; Triolo, M.; Girgis, J.; Chwastek, D.; Larrigan, S.; Feige, P.; Fujita, R.; Crist, C.; Rudnicki, M. A.; Burelle, Y.; Khacho, M. The Mitochondrial Protein OPA1 Regulates the Quiescent State of Adult Muscle Stem Cells. *Cell Stem Cell* **2022**, *29* (9), 1315-1332.e9. https://doi.org/10.1016/j.stem.2022.07.010.
(51) Troy, A.; Cadwallader, A. B.; Fedorov, Y.; Tyner, K.; Tanaka, K. K.; Olwin, B. B. Coordination of Satellite Cell Activation and Self-Renewal by Par-Complex-Dependent Asymmetric Activation of P38α/β MAPK. *Cell Stem Cell* **2012**, *11* (4), 541–553. https://doi.org/10.1016/j.stem.2012.05.025.
(52) Fu, X.; Zhuang, C.; Hu, P. Regulation of Muscle Stem Cell Fate. *Cell Regeneration* **2022**, *11* (1), 40. https://doi.org/10.1186/s13619-022-00142-7.
(53) Gugliuzza, M. V.; Crist, C. Muscle Stem Cell Adaptations to Cellular and Environmental Stress. *Skeletal Muscle* **2022**, *12* (1), 5. https://doi.org/10.1186/s13395-022-00289-6.
(54) Schmidt, M.; Schüler, S. C.; Hüttner, S. S.; von Eyss, B.; von Maltzahn, J. Adult Stem Cells at Work: Regenerating Skeletal Muscle. *Cell. Mol. Life Sci.* **2019**, *76* (13), 2559–2570. https://doi.org/10.1007/s00018-019-03093-6.
(55) Seale, P.; Sabourin, L. A.; Girgis-Gabardo, A.; Mansouri, A.; Gruss, P.; Rudnicki, M. A. Pax7 Is Required for the Specification of Myogenic Satellite Cells. *Cell* **2000**, *102* (6), 777–786. https://doi.org/10.1016/S0092-8674(00)00066-0.
(56) Brack, A. S.; Conboy, I. M.; Conboy, M. J.; Shen, J.; Rando, T. A. A Temporal Switch from Notch to Wnt Signaling in Muscle Stem Cells Is Necessary for Normal Adult Myogenesis. *Cell Stem Cell* **2008**, *2* (1), 50–59. https://doi.org/10.1016/j.stem.2007.10.006.
(57) Tierney, M. T.; Sacco, A. Satellite Cell Heterogeneity in Skeletal Muscle Homeostasis. *Trends Cell Biol* **2016**, *26* (6), 434–444. https://doi.org/10.1016/j.tcb.2016.02.004.

(58) Shea, K. L.; Xiang, W.; LaPorta, V. S.; Licht, J. D.; Keller, C.; Basson, M. A.; Brack, A. S. Sprouty1 Regulates Reversible Quiescence of a Self-Renewing Adult Muscle Stem Cell Pool during Regeneration. *Cell Stem Cell* **2010**, *6* (2), 117–129. https://doi.org/10.1016/j.stem.2009.12.015.
(59) Bjornson, C. R. R.; Cheung, T. H.; Liu, L.; Tripathi, P. V.; Steeper, K. M.; Rando, T. A. Notch Signaling Is Necessary to Maintain Quiescence in Adult Muscle Stem Cells. *Stem Cells* **2012**, *30* (2), 232–242. https://doi.org/10.1002/stem.773.
(60) Zwetsloot, K. A.; Childs, T. E.; Gilpin, L. T.; Booth, F. W. Non-Passaged Muscle Precursor Cells from 32-Month Old Rat Skeletal Muscle Have Delayed Proliferation and Differentiation. *Cell Proliferation* **2013**, *46* (1), 45–57. https://doi.org/10.1111/cpr.12007.
(61) Sousa-Victor, P.; Perdiguero, E.; Muñoz-Cánoves, P. Geroconversion of Aged Muscle Stem Cells under Regenerative Pressure. *Cell Cycle* **2014**, *13* (20), 3183–3190. https://doi.org/10.4161/15384101.2014.965072.
(62) Lilja, K. C.; Zhang, N.; Magli, A.; Gunduz, V.; Bowman, C. J.; Arpke, R. W.; Darabi, R.; Kyba, M.; Perlingeiro, R.; Dynlacht, B. D. Pax7 Remodels the Chromatin Landscape in Skeletal Muscle Stem Cells. *PLOS ONE* **2017**, *12* (4), e0176190. https://doi.org/10.1371/journal.pone.0176190.
(63) Zhang, N.; Mendieta-Esteban, J.; Magli, A.; Lilja, K. C.; Perlingeiro, R. C. R.; Marti-Renom, M. A.; Tsirigos, A.; Dynlacht, B. D. Muscle Progenitor Specification and Myogenic Differentiation Are Associated with Changes in Chromatin Topology. *Nat Commun* **2020**, *11* (1), 6222. https://doi.org/10.1038/s41467-020-19999-w.
(64) Dey, B. K.; Gagan, J.; Dutta, A. miR-206 and -486 Induce Myoblast Differentiation by Downregulating Pax7. *Molecular and Cellular Biology* **2011**, *31* (1), 203–214. https://doi.org/10.1128/MCB.01009-10.
(65) *Satellite Cells and the Muscle Stem Cell Niche | Physiological Reviews | American Physiological Society*. https://journals.physiology.org/doi/full/10.1152/physrev.00043.2011 (accessed 2025-02-21).
(66) Hasty, P.; Bradley, A.; Morris, J. H.; Edmondson, D. G.; Venuti, J. M.; Olson, E. N.; Klein, W. H. Muscle Deficiency and Neonatal Death in Mice with a Targeted Mutation in the Myogenin Gene. *Nature* **1993**, *364* (6437), 501–506. https://doi.org/10.1038/364501a0.
(67) Nabeshima, Y.; Hanaoka, K.; Hayasaka, M.; Esuml, E.; Li, S.; Nonaka, I.; Nabeshima, Y. Myogenin Gene Disruption Results in Perinatal Lethality Because of Severe Muscle Defect. *Nature* **1993**, *364* (6437), 532–535. https://doi.org/10.1038/364532a0.
(68) Weintraub, H.; Davis, R.; Tapscott, S.; Thayer, M.; Krause, M.; Benezra, R.; Blackwell, T. K.; Turner, D.; Rupp, R.; Hollenberg, S.; Zhuang, Y.; Lassar, A. The myoD Gene Family: Nodal Point During Specification of the Muscle Cell Lineage. *Science* **1991**, *251* (4995), 761–766. https://doi.org/10.1126/science.1846704.
(69) Rhodes, S. J.; Konieczny, S. F. Identification of MRF4: A New Member of the Muscle Regulatory Factor Gene Family. *Genes Dev.* **1989**, *3* (12b), 2050–2061. https://doi.org/10.1101/gad.3.12b.2050.
(70) Sartore, S.; Gorza, L.; Schiaffino, S. Fetal Myosin Heavy Chains in Regenerating Muscle. *Nature* **1982**, *298* (5871), 294–296. https://doi.org/10.1038/298294a0.
(71) Schiaffino, S.; Gorza, L.; Dones, I.; Cornelio, F.; Sartore, S. Fetal Myosin Immunoreactivity in Human Dystrophic Muscle. *Muscle Nerve* **1986**, *9* (1), 51–58. https://doi.org/10.1002/mus.880090108.

(72) Schiaffino, S.; Rossi, A. C.; Smerdu, V.; Leinwand, L. A.; Reggiani, C. Developmental Myosins: Expression Patterns and Functional Significance. *Skeletal Muscle* **2015**, *5* (1), 22. https://doi.org/10.1186/s13395-015-0046-6.
(73) Baumgartner, R. N.; Waters, D. L.; Gallagher, D.; Morley, J. E.; Garry, P. J. Predictors of Skeletal Muscle Mass in Elderly Men and Women. *Mechanisms of Ageing and Development* **1999**, *107* (2), 123–136. https://doi.org/10.1016/S0047-6374(98)00130-4.
(74) Fielding, R. A.; Vellas, B.; Evans, W. J.; Bhasin, S.; Morley, J. E.; Newman, A. B.; Kan, G. A. van; Andrieu, S.; Bauer, J.; Breuille, D.; Cederholm, T.; Chandler, J.; Meynard, C. D.; Donini, L.; Harris, T.; Kannt, A.; Guibert, F. K.; Onder, G.; Papanicolaou, D.; Rolland, Y.; Rooks, D.; Sieber, C.; Souhami, E.; Verlaan, S.; Zamboni, M. Sarcopenia: An Undiagnosed Condition in Older Adults. Current Consensus Definition: Prevalence, Etiology, and Consequences. International Working Group on Sarcopenia. *Journal of the American Medical Directors Association* **2011**, *12* (4), 249–256. https://doi.org/10.1016/j.jamda.2011.01.003.
(75) Metter, E. J.; Talbot, L. A.; Schrager, M.; Conwit, R. A. Arm-Cranking Muscle Power and Arm Isometric Muscle Strength Are Independent Predictors of All-Cause Mortality in Men. *Journal of Applied Physiology* **2004**, *96* (2), 814–821. https://doi.org/10.1152/japplphysiol.00370.2003.
(76) Cruz-Jentoft, A. J.; Sayer, A. A. Sarcopenia. *The Lancet* **2019**, *393* (10191), 2636–2646. https://doi.org/10.1016/S0140-6736(19)31138-9.
(77) Vandervoort, A. A.; Symons, T. B. Functional and Metabolic Consequences of Sarcopenia. *Can. J. Appl. Physiol.* **2001**, *26* (1), 90–101. https://doi.org/10.1139/h01-007.
(78) Lexell, J.; Taylor, C. C.; Sjöström, M. What Is the Cause of the Ageing Atrophy?: Total Number, Size and Proportion of Different Fiber Types Studied in Whole Vastus Lateralis Muscle from 15- to 83-Year-Old Men. *Journal of the Neurological Sciences* **1988**, *84* (2), 275–294. https://doi.org/10.1016/0022-510X(88)90132-3.
(79) Evans, W. J.; Lexell, J. Human Aging, Muscle Mass, and Fiber Type Composition. *The Journals of Gerontology: Series A* **1995**, *50A* (Special_Issue), 11–16. https://doi.org/10.1093/gerona/50A.Special_Issue.11.
(80) Campbell, M. J.; McComas, A. J.; Petito, F. Physiological Changes in Ageing Muscles. *Journal of Neurology, Neurosurgery & Psychiatry* **1973**, *36* (2), 174–182. https://doi.org/10.1136/jnnp.36.2.174.
(81) Urbanchek, M. G.; Picken, E. B.; Kalliainen, L. K.; Kuzon, W. M. Specific Force Deficit in Skeletal Muscles of Old Rats Is Partially Explained by the Existence of Denervated Muscle Fibers. *J Gerontol A Biol Sci Med Sci* **2001**, *56* (5), B191-197. https://doi.org/10.1093/gerona/56.5.b191.
(82) Booth, F. W.; Weeden, S. H.; Tseng, B. S. Effect of Aging on Human Skeletal Muscle and Motor Function. *Med Sci Sports Exerc* **1994**, *26* (5), 556–560.
(83) Marzetti, E.; Wohlgemuth, S. E.; Lees, H. A.; Chung, H.-Y.; Giovannini, S.; Leeuwenburgh, C. Age-Related Activation of Mitochondrial Caspase-Independent Apoptotic Signaling in Rat Gastrocnemius Muscle. *Mechanisms of Ageing and Development* **2008**, *129* (9), 542–549. https://doi.org/10.1016/j.mad.2008.05.005.
(84) Siu, P. M.; Pistilli, E. E.; Alway, S. E. Age-Dependent Increase in Oxidative Stress in Gastrocnemius Muscle with Unloading. *Journal of Applied Physiology* **2008**, *105* (6), 1695–1705. https://doi.org/10.1152/japplphysiol.90800.2008.

(85) Carter, C. S.; Hofer, T.; Seo, A. Y.; Leeuwenburgh, C. Molecular Mechanisms of Life- and Health-Span Extension: Role of Calorie Restriction and Exercise Intervention. *Appl. Physiol. Nutr. Metab.* **2007**, *32* (5), 954–966. https://doi.org/10.1139/H07-085.
(86) Bouché, M.; Muñoz-Cánoves, P.; Rossi, F.; Coletti, D. Inflammation in Muscle Repair, Aging, and Myopathies. *BioMed Research International* **2014**, *2014* (1), 821950. https://doi.org/10.1155/2014/821950.
(87) Sousa-Victor, P.; Gutarra, S.; García-Prat, L.; Rodriguez-Ubreva, J.; Ortet, L.; Ruiz-Bonilla, V.; Jardí, M.; Ballestar, E.; González, S.; Serrano, A. L.; Perdiguero, E.; Muñoz-Cánoves, P. Geriatric Muscle Stem Cells Switch Reversible Quiescence into Senescence. *Nature* **2014**, *506* (7488), 316–321. https://doi.org/10.1038/nature13013.
(88) Price, F. D.; von Maltzahn, J.; Bentzinger, C. F.; Dumont, N. A.; Yin, H.; Chang, N. C.; Wilson, D. H.; Frenette, J.; Rudnicki, M. A. Inhibition of JAK-STAT Signaling Stimulates Adult Satellite Cell Function. *Nat Med* **2014**, *20* (10), 1174–1181. https://doi.org/10.1038/nm.3655.
(89) Porpiglia, E.; Mai, T.; Kraft, P.; Holbrook, C. A.; de Morree, A.; Gonzalez, V. D.; Hilgendorf, K. I.; Frésard, L.; Trejo, A.; Bhimaraju, S.; Jackson, P. K.; Fantl, W. J.; Blau, H. M. Elevated CD47 Is a Hallmark of Dysfunctional Aged Muscle Stem Cells That Can Be Targeted to Augment Regeneration. *Cell Stem Cell* **2022**, *29* (12), 1653-1668.e8. https://doi.org/10.1016/j.stem.2022.10.009.
(90) *SATELLITE CELL OF SKELETAL MUSCLE FIBERS - PMC*. https://pmc.ncbi.nlm.nih.gov/articles/PMC2225012/ (accessed 2025-02-20).
(91) Bernet, J. D.; Doles, J. D.; Hall, J. K.; Kelly Tanaka, K.; Carter, T. A.; Olwin, B. B. P38 MAPK Signaling Underlies a Cell-Autonomous Loss of Stem Cell Self-Renewal in Skeletal Muscle of Aged Mice. *Nat Med* **2014**, *20* (3), 265–271. https://doi.org/10.1038/nm.3465.
(92) Blau, H. M.; Cosgrove, B. D.; Ho, A. T. V. The Central Role of Muscle Stem Cells in Regenerative Failure with Aging. *Nat Med* **2015**, *21* (8), 854–862. https://doi.org/10.1038/nm.3918.
(93) Zeng, W.; Zhang, W.; Tse, E. H. Y.; Liu, J.; Dong, A.; Lam, K. S. W.; Luan, S.; Kung, W. H.; Chan, T. C.; Cheung, T. H. Restoration of CPEB4 Prevents Muscle Stem Cell Senescence during Aging. *Developmental Cell* **2023**, *58* (15), 1383-1398.e6. https://doi.org/10.1016/j.devcel.2023.05.012.
(94) Buckingham, M.; Relaix, F. The Role of Pax Genes in the Development of Tissues and Organs: Pax3 and Pax7 Regulate Muscle Progenitor Cell Functions. *Annual Review of Cell and Developmental Biology* **2007**, *23* (Volume 23, 2007), 645–673. https://doi.org/10.1146/annurev.cellbio.23.090506.123438.
(95) Collins, C. A.; Gnocchi, V. F.; White, R. B.; Boldrin, L.; Perez-Ruiz, A.; Relaix, F.; Morgan, J. E.; Zammit, P. S. Integrated Functions of Pax3 and Pax7 in the Regulation of Proliferation, Cell Size and Myogenic Differentiation. *PLOS ONE* **2009**, *4* (2), e4475. https://doi.org/10.1371/journal.pone.0004475.
(96) *TNF/p38α/Polycomb Signaling to Pax7 Locus in Satellite Cells Links Inflammation to the Epigenetic Control of Muscle Regeneration: Cell Stem Cell*. https://www.cell.com/cell-stem-cell/fulltext/S1934-5909(10)00435-2?_returnURL=https%3A%2F%2Flinkinghub.elsevier.com%2Fretrieve%2Fpii%2FS1934590910004352%3Fshowall%3Dtrue (accessed 2025-02-18).

(97) López-Otín, C.; Blasco, M. A.; Partridge, L.; Serrano, M.; Kroemer, G. Hallmarks of Aging: An Expanding Universe. *Cell* **2023**, *186* (2), 243–278. https://doi.org/10.1016/j.cell.2022.11.001.
(98) *Frontiers | Age- and Tissue-Specific Expression of Senescence Biomarkers in Mice*. https://www.frontiersin.org/journals/genetics/articles/10.3389/fgene.2018.00059/full (accessed 2025-02-18).
(99) Dimri, G. P.; Lee, X.; Basile, G.; Acosta, M.; Scott, G.; Roskelley, C.; Medrano, E. E.; Linskens, M.; Rubelj, I.; Pereira-Smith, O. A Biomarker That Identifies Senescent Human Cells in Culture and in Aging Skin in Vivo. *Proceedings of the National Academy of Sciences* **1995**, *92* (20), 9363–9367. https://doi.org/10.1073/pnas.92.20.9363.
(100) Herbig, U.; Ferreira, M.; Condel, L.; Carey, D.; Sedivy, J. M. Cellular Senescence in Aging Primates. *Science* **2006**, *311* (5765), 1257–1257. https://doi.org/10.1126/science.1122446.
(101) Chen, Z.; Trotman, L. C.; Shaffer, D.; Lin, H.-K.; Dotan, Z. A.; Niki, M.; Koutcher, J. A.; Scher, H. I.; Ludwig, T.; Gerald, W.; Cordon-Cardo, C.; Paolo Pandolfi, P. Crucial Role of P53-Dependent Cellular Senescence in Suppression of Pten-Deficient Tumorigenesis. *Nature* **2005**, *436* (7051), 725–730. https://doi.org/10.1038/nature03918.
(102) Lin, H.-K.; Chen, Z.; Wang, G.; Nardella, C.; Lee, S.-W.; Chan, C.-H.; Yang, W.-L.; Wang, J.; Egia, A.; Nakayama, K. I.; Cordon-Cardo, C.; Teruya-Feldstein, J.; Pandolfi, P. P. Skp2 Targeting Suppresses Tumorigenesis by Arf-P53-Independent Cellular Senescence. *Nature* **2010**, *464* (7287), 374–379. https://doi.org/10.1038/nature08815.
(103) Li, F.; Huangyang, P.; Burrows, M.; Guo, K.; Riscal, R.; Godfrey, J.; Lee, K. E.; Lin, N.; Lee, P.; Blair, I. A.; Keith, B.; Li, B.; Simon, M. C. FBP1 Loss Disrupts Liver Metabolism and Promotes Tumorigenesis through a Hepatic Stellate Cell Senescence Secretome. *Nat Cell Biol* **2020**, *22* (6), 728–739. https://doi.org/10.1038/s41556-020-0511-2.
(104) Sharpless, N. E.; Sherr, C. J. Forging a Signature of in Vivo Senescence. *Nat Rev Cancer* **2015**, *15* (7), 397–408. https://doi.org/10.1038/nrc3960.
(105) Hayflick, L.; Moorhead, P. S. The Serial Cultivation of Human Diploid Cell Strains. *Experimental Cell Research* **1961**, *25* (3), 585–621. https://doi.org/10.1016/0014-4827(61)90192-6.
(106) Muñoz-Espín, D.; Serrano, M. Cellular Senescence: From Physiology to Pathology. *Nat Rev Mol Cell Biol* **2014**, *15* (7), 482–496. https://doi.org/10.1038/nrm3823.
(107) Wiley, C. D.; Velarde, M. C.; Lecot, P.; Liu, S.; Sarnoski, E. A.; Freund, A.; Shirakawa, K.; Lim, H. W.; Davis, S. S.; Ramanathan, A.; Gerencser, A. A.; Verdin, E.; Campisi, J. Mitochondrial Dysfunction Induces Senescence with a Distinct Secretory Phenotype. *Cell Metabolism* **2016**, *23* (2), 303–314. https://doi.org/10.1016/j.cmet.2015.11.011.
(108) Acosta, J. C.; Banito, A.; Wuestefeld, T.; Georgilis, A.; Janich, P.; Morton, J. P.; Athineos, D.; Kang, T.-W.; Lasitschka, F.; Andrulis, M.; Pascual, G.; Morris, K. J.; Khan, S.; Jin, H.; Dharmalingam, G.; Snijders, A. P.; Carroll, T.; Capper, D.; Pritchard, C.; Inman, G. J.; Longerich, T.; Sansom, O. J.; Benitah, S. A.; Zender, L.; Gil, J. A Complex Secretory Program Orchestrated by the Inflammasome Controls Paracrine Senescence. *Nat Cell Biol* **2013**, *15* (8), 978–990. https://doi.org/10.1038/ncb2784.
(109) Wang, C.; Jurk, D.; Maddick, M.; Nelson, G.; Martin-Ruiz, C.; Von Zglinicki, T. DNA Damage Response and Cellular Senescence in Tissues of Aging Mice. *Aging Cell* **2009**, *8* (3), 311–323. https://doi.org/10.1111/j.1474-9726.2009.00481.x.

(110) *Small molecule compounds that induce cellular senescence - Petrova - 2016 - Aging Cell - Wiley Online Library*. https://onlinelibrary.wiley.com/doi/10.1111/acel.12518 (accessed 2025-02-18).
(111)Hernandez-Segura, A.; Nehme, J.; Demaria, M. Hallmarks of Cellular Senescence. *Trends in Cell Biology* **2018**, *28* (6), 436–453. https://doi.org/10.1016/j.tcb.2018.02.001.
(112) Kamal, M.; Shanmuganathan, M.; Kroezen, Z.; Joanisse, S.; Britz-McKibbin, P.; Parise, G. Senescent Myoblasts Exhibit an Altered Exometabolome That Is Linked to Senescence-Associated Secretory Phenotype (SASP) Signalling. *American Journal of Physiology-Cell Physiology* **2024**. https://doi.org/10.1152/ajpcell.00880.2024.
(113) Mohamad Kamal, N. S.; Safuan, S.; Shamsuddin, S.; Foroozandeh, P. Aging of the Cells: Insight into Cellular Senescence and Detection Methods. *European Journal of Cell Biology* **2020**, *99* (6), 151108. https://doi.org/10.1016/j.ejcb.2020.151108.
(114) Korotchkina, L. G.; Leontieva, O. V.; Bukreeva, E. I.; Demidenko, Z. N.; Gudkov, A. V.; Blagosklonny, M. V. The Choice between P53-Induced Senescence and Quiescence Is Determined in Part by the mTOR Pathway. *Aging* **2010**, *2* (6), 344–352. https://doi.org/10.18632/aging.100160.
(115) Ge, Y.; Miao, Y.; Gur-Cohen, S.; Gomez, N.; Yang, H.; Nikolova, M.; Polak, L.; Hu, Y.; Verma, A.; Elemento, O.; Krueger, J. G.; Fuchs, E. The Aging Skin Microenvironment Dictates Stem Cell Behavior. *Proceedings of the National Academy of Sciences* **2020**, *117* (10), 5339–5350. https://doi.org/10.1073/pnas.1901720117.
(116) Conboy, I. M.; Rando, T. A. Aging, Stem Cells and Tissue Regeneration: Lessons from Muscle. *Cell Cycle* **2005**, *4* (3), 407–410. https://doi.org/10.4161/cc.4.3.1518.
(117) Chandel, N. S.; Jasper, H.; Ho, T. T.; Passegué, E. Metabolic Regulation of Stem Cell Function in Tissue Homeostasis and Organismal Ageing. *Nat Cell Biol* **2016**, *18* (8), 823–832. https://doi.org/10.1038/ncb3385.
(118) Alt, E. U.; Senst, C.; Murthy, S. N.; Slakey, D. P.; Dupin, C. L.; Chaffin, A. E.; Kadowitz, P. J.; Izadpanah, R. Aging Alters Tissue Resident Mesenchymal Stem Cell Properties. *Stem Cell Research* **2012**, *8* (2), 215–225. https://doi.org/10.1016/j.scr.2011.11.002.
(119) Carlson, M. E.; Hsu, M.; Conboy, I. M. Imbalance between pSmad3 and Notch Induces CDK Inhibitors in Old Muscle Stem Cells. *Nature* **2008**, *454* (7203), 528–532. https://doi.org/10.1038/nature07034.
(120) Sousa-Victor, P.; García-Prat, L.; Muñoz-Cánoves, P. Control of Satellite Cell Function in Muscle Regeneration and Its Disruption in Ageing. *Nat Rev Mol Cell Biol* **2022**, *23* (3), 204–226. https://doi.org/10.1038/s41580-021-00421-2.
(121) García-Prat, L.; Martínez-Vicente, M.; Perdiguero, E.; Ortet, L.; Rodríguez-Ubreva, J.; Rebollo, E.; Ruiz-Bonilla, V.; Gutarra, S.; Ballestar, E.; Serrano, A. L.; Sandri, M.; Muñoz-Cánoves, P. Autophagy Maintains Stemness by Preventing Senescence. *Nature* **2016**, *529* (7584), 37–42. https://doi.org/10.1038/nature16187.
(122) Baker, D. J.; Perez-Terzic, C.; Jin, F.; Pitel, K. S.; Niederländer, N. J.; Jeganathan, K.; Yamada, S.; Reyes, S.; Rowe, L.; Hiddinga, H. J.; Eberhardt, N. L.; Terzic, A.; van Deursen, J. M. Opposing Roles for p16Ink4a and p19Arf in Senescence and Ageing Caused by BubR1 Insufficiency. *Nat Cell Biol* **2008**, *10* (7), 825–836. https://doi.org/10.1038/ncb1744.
(123) Baker, D. J.; Wijshake, T.; Tchkonia, T.; LeBrasseur, N. K.; Childs, B. G.; van de Sluis, B.; Kirkland, J. L.; van Deursen, J. M. Clearance of p16Ink4a-Positive Senescent Cells

Delays Ageing-Associated Disorders. *Nature* **2011**, *479* (7372), 232–236. https://doi.org/10.1038/nature10600.
(124) Zhang, P.; Wong, C.; Liu, D.; Finegold, M.; Harper, J. W.; Elledge, S. J. p21CIP1 and p57KIP2 Control Muscle Differentiation at the Myogenin Step. *Genes Dev.* **1999**, *13* (2), 213–224.
(125) Moiseeva, V.; Cisneros, A.; Sica, V.; Deryagin, O.; Lai, Y.; Jung, S.; Andrés, E.; An, J.; Segalés, J.; Ortet, L.; Lukesova, V.; Volpe, G.; Benguria, A.; Dopazo, A.; Benitah, S. A.; Urano, Y.; del Sol, A.; Esteban, M. A.; Ohkawa, Y.; Serrano, A. L.; Perdiguero, E.; Muñoz-Cánoves, P. Senescence Atlas Reveals an Aged-like Inflamed Niche That Blunts Muscle Regeneration. *Nature* **2023**, *613* (7942), 169–178. https://doi.org/10.1038/s41586-022-05535-x.
(126) Englund, D. A.; Jolliffe, A.; Aversa, Z.; Zhang, X.; Sturmlechner, I.; Sakamoto, A. E.; Zeidler, J. D.; Warner, G. M.; McNinch, C.; White, T. A.; Chini, E. N.; Baker, D. J.; van Deursen, J. M.; LeBrasseur, N. K. P21 Induces a Senescence Program and Skeletal Muscle Dysfunction. *Molecular Metabolism* **2023**, *67*, 101652. https://doi.org/10.1016/j.molmet.2022.101652.
(127) Robinson, D. C. L.; Ritso, M.; Nelson, G. M.; Mokhtari, Z.; Nakka, K.; Bandukwala, H.; Goldman, S. R.; Park, P. J.; Mounier, R.; Chazaud, B.; Brand, M.; Rudnicki, M. A.; Adelman, K.; Dilworth, F. J. Negative Elongation Factor Regulates Muscle Progenitor Expansion for Efficient Myofiber Repair and Stem Cell Pool Repopulation. *Developmental Cell* **2021**, *56* (7), 1014-1029.e7. https://doi.org/10.1016/j.devcel.2021.02.025.
(128) Liu, L.; Charville, G. W.; Cheung, T. H.; Yoo, B.; Santos, P. J.; Schroeder, M.; Rando, T. A. Impaired Notch Signaling Leads to a Decrease in P53 Activity and Mitotic Catastrophe in Aged Muscle Stem Cells. *Cell Stem Cell* **2018**, *23* (4), 544-556.e4. https://doi.org/10.1016/j.stem.2018.08.019.
(129) Diao, Y.; Guo, X.; Li, Y.; Sun, K.; Lu, L.; Jiang, L.; Fu, X.; Zhu, H.; Sun, H.; Wang, H.; Wu, Z. Pax3/7BP Is a Pax7- and Pax3-Binding Protein That Regulates the Proliferation of Muscle Precursor Cells by an Epigenetic Mechanism. *Cell Stem Cell* **2012**, *11* (2), 231–241. https://doi.org/10.1016/j.stem.2012.05.022.
(130) Senior, A. E. ATP Synthesis by Oxidative Phosphorylation. *Physiological Reviews* **1988**, *68* (1), 177–231. https://doi.org/10.1152/physrev.1988.68.1.177.
(131) Lesnefsky, E. J.; Moghaddas, S.; Tandler, B.; Kerner, J.; Hoppel, C. L. Mitochondrial Dysfunction in Cardiac Disease: Ischemia–Reperfusion, Aging, and Heart Failure. *Journal of Molecular and Cellular Cardiology* **2001**, *33* (6), 1065–1089. https://doi.org/10.1006/jmcc.2001.1378.
(132) Wallace, D. C. Mitochondrial Defects in Cardiomyopathy and Neuromuscular Disease. *American Heart Journal* **2000**, *139* (2, Supplement 2), s70–s85. https://doi.org/10.1067/mhj.2000.103934.
(133) Sugioka, K.; Nakano, M.; Totsune-Nakano, H.; Minakami, H.; Tero-Kubota, S.; Ikegami, Y. Mechanism of O−2 Generation in Reduction and Oxidation Cycle of Ubiquinones in a Model of Mitochondrial Electron Transport Systems. *Biochimica et Biophysica Acta (BBA) - Bioenergetics* **1988**, *936* (3), 377–385. https://doi.org/10.1016/0005-2728(88)90014-X.
(134) Turrens, J. F.; Boveris, A. Generation of Superoxide Anion by the NADH Dehydrogenase of Bovine Heart Mitochondria. *Biochemical Journal* **1980**, *191* (2), 421–427. https://doi.org/10.1042/bj1910421.

(135) Chen, Q.; Vazquez, E. J.; Moghaddas, S.; Hoppel, C. L.; Lesnefsky, E. J. Production of Reactive Oxygen Species by Mitochondria: CENTRAL ROLE OF COMPLEX III*. *Journal of Biological Chemistry* **2003**, *278* (38), 36027–36031. https://doi.org/10.1074/jbc.M304854200.
(136) Triolo, M.; Baker, N.; Agarwal, S.; Larionov, N.; Podinić, T.; Khacho, M. Optic Atrophy 1 Mediates Muscle Differentiation by Promoting a Metabolic Switch via the Supercomplex Assembly Factor SCAF1. *iScience* **2024**, *27* (3), 109164. https://doi.org/10.1016/j.isci.2024.109164.
(137) Cavalcanti, J. H. F.; Esteves-Ferreira, A. A.; Quinhones, C. G. S.; Pereira-Lima, I. A.; Nunes-Nesi, A.; Fernie, A. R.; Araújo, W. L. Evolution and Functional Implications of the Tricarboxylic Acid Cycle as Revealed by Phylogenetic Analysis. *Genome Biology and Evolution* **2014**, *6* (10), 2830–2848. https://doi.org/10.1093/gbe/evu221.
(138) Arnold, P. K.; Finley, L. W. S. Regulation and Function of the Mammalian Tricarboxylic Acid Cycle. *J Biol Chem* **2022**, *299* (2), 102838. https://doi.org/10.1016/j.jbc.2022.102838.
(139) Eniafe, J.; Jiang, S. The Functional Roles of TCA Cycle Metabolites in Cancer. *Oncogene* **2021**, *40* (19), 3351–3363. https://doi.org/10.1038/s41388-020-01639-8.
(140) Boroughs, L. K.; DeBerardinis, R. J. Metabolic Pathways Promoting Cancer Cell Survival and Growth. *Nat Cell Biol* **2015**, *17* (4), 351–359. https://doi.org/10.1038/ncb3124.
(141) Wellen, K. E.; Thompson, C. B. A Two-Way Street: Reciprocal Regulation of Metabolism and Signalling. *Nat Rev Mol Cell Biol* **2012**, *13* (4), 270–276. https://doi.org/10.1038/nrm3305.
(142) Tsogtbaatar, E.; Landin, C.; Minter-Dykhouse, K.; Folmes, C. D. L. Energy Metabolism Regulates Stem Cell Pluripotency. *Front. Cell Dev. Biol.* **2020**, *8*. https://doi.org/10.3389/fcell.2020.00087.
(143) Guo, D.; He, H.; Meng, Y.; Luo, S.; Lu, Z. Determiners of Cell Fates: The Tricarboxylic Acid Cycle versus the Citrate-Malate Shuttle. *Protein & Cell* **2023**, *14* (3), 162–164. https://doi.org/10.1093/procel/pwac026.
(144) Arnold, P. K.; Jackson, B. T.; Paras, K. I.; Brunner, J. S.; Hart, M. L.; Newsom, O. J.; Alibeckoff, S. P.; Endress, J.; Drill, E.; Sullivan, L. B.; Finley, L. W. S. A Non-Canonical Tricarboxylic Acid Cycle Underlies Cellular Identity. *Nature* **2022**, *603* (7901), 477–481. https://doi.org/10.1038/s41586-022-04475-w.
(145) Brillo, V.; Chieregato, L.; Leanza, L.; Muccioli, S.; Costa, R. Mitochondrial Dynamics, ROS, and Cell Signaling: A Blended Overview. *Life* **2021**, *11* (4), 332. https://doi.org/10.3390/life11040332.
(146) Yu, B.; Ma, J.; Li, J.; Wang, D.; Wang, Z.; Wang, S. Mitochondrial Phosphatase PGAM5 Modulates Cellular Senescence by Regulating Mitochondrial Dynamics. *Nat Commun* **2020**, *11* (1), 2549. https://doi.org/10.1038/s41467-020-16312-7.
(147) Mishra, P.; Chan, D. C. Mitochondrial Dynamics and Inheritance during Cell Division, Development and Disease. *Nat Rev Mol Cell Biol* **2014**, *15* (10), 634–646. https://doi.org/10.1038/nrm3877.
(148) Deng, H.; Dodson, M. W.; Huang, H.; Guo, M. The Parkinson's Disease Genes Pink1 and Parkin Promote Mitochondrial Fission and/or Inhibit Fusion in Drosophila. *Proceedings of the National Academy of Sciences* **2008**, *105* (38), 14503–14508. https://doi.org/10.1073/pnas.0803998105.

(149) Chen, H.; Detmer, S. A.; Ewald, A. J.; Griffin, E. E.; Fraser, S. E.; Chan, D. C. Mitofusins Mfn1 and Mfn2 Coordinately Regulate Mitochondrial Fusion and Are Essential for Embryonic Development. *J Cell Biol* **2003**, *160* (2), 189–200. https://doi.org/10.1083/jcb.200211046.
(150) Cao, Y.-L.; Meng, S.; Chen, Y.; Feng, J.-X.; Gu, D.-D.; Yu, B.; Li, Y.-J.; Yang, J.-Y.; Liao, S.; Chan, D. C.; Gao, S. MFN1 Structures Reveal Nucleotide-Triggered Dimerization Critical for Mitochondrial Fusion. *Nature* **2017**, *542* (7641), 372–376. https://doi.org/10.1038/nature21077.
(151) Frezza, C.; Cipolat, S.; Brito, O. M. de; Micaroni, M.; Beznoussenko, G. V.; Rudka, T.; Bartoli, D.; Polishuck, R. S.; Danial, N. N.; Strooper, B. D.; Scorrano, L. OPA1 Controls Apoptotic Cristae Remodeling Independently from Mitochondrial Fusion. *Cell* **2006**, *126* (1), 177–189. https://doi.org/10.1016/j.cell.2006.06.025.
(152) Fry, M. Y.; Navarro, P. P.; Hakim, P.; Ananda, V. Y.; Qin, X.; Landoni, J. C.; Rath, S.; Inde, Z.; Lugo, C. M.; Luce, B. E.; Ge, Y.; McDonald, J. L.; Ali, I.; Ha, L. L.; Kleinstiver, B. P.; Chan, D. C.; Sarosiek, K. A.; Chao, L. H. In Situ Architecture of Opa1-Dependent Mitochondrial Cristae Remodeling. bioRxiv November 9, 2023, p 2023.01.16.524176. https://doi.org/10.1101/2023.01.16.524176.
(153) Olichon, A.; Baricault, L.; Gas, N.; Guillou, E.; Valette, A.; Belenguer, P.; Lenaers, G. Loss of OPA1 Perturbates the Mitochondrial Inner Membrane Structure and Integrity, Leading to Cytochrome c Release and Apoptosis *. *Journal of Biological Chemistry* **2003**, *278* (10), 7743–7746. https://doi.org/10.1074/jbc.C200677200.
(154) Ge, Y.; Shi, X.; Boopathy, S.; McDonald, J.; Smith, A. W.; Chao, L. H. Two Forms of Opa1 Cooperate to Complete Fusion of the Mitochondrial Inner-Membrane. *eLife* **2020**, *9*, e50973. https://doi.org/10.7554/eLife.50973.
(155) Gilkerson, R.; De La Torre, P.; St. Vallier, S. Mitochondrial OMA1 and OPA1 as Gatekeepers of Organellar Structure/Function and Cellular Stress Response. *Front. Cell Dev. Biol.* **2021**, *9*. https://doi.org/10.3389/fcell.2021.626117.
(156) Ban, T.; Heymann, J. A. W.; Song, Z.; Hinshaw, J. E.; Chan, D. C. OPA1 Disease Alleles Causing Dominant Optic Atrophy Have Defects in Cardiolipin-Stimulated GTP Hydrolysis and Membrane Tubulation. *Human Molecular Genetics* **2010**, *19* (11), 2113–2122. https://doi.org/10.1093/hmg/ddq088.
(157) Zhang, D.; Zhang, Y.; Ma, J.; Zhu, C.; Niu, T.; Chen, W.; Pang, X.; Zhai, Y.; Sun, F. Cryo-EM Structures of S-OPA1 Reveal Its Interactions with Membrane and Changes upon Nucleotide Binding. *eLife* **2020**, *9*, e50294. https://doi.org/10.7554/eLife.50294.
(158) Abrisch, R. G.; Gumbin, S. C.; Wisniewski, B. T.; Lackner, L. L.; Voeltz, G. K. Fission and Fusion Machineries Converge at ER Contact Sites to Regulate Mitochondrial Morphology. *Journal of Cell Biology* **2020**, *219* (4), e201911122. https://doi.org/10.1083/jcb.201911122.
(159) Adaniya, S. M.; O-Uchi, J.; Cypress, M. W.; Kusakari, Y.; Jhun, B. S. Posttranslational Modifications of Mitochondrial Fission and Fusion Proteins in Cardiac Physiology and Pathophysiology. *American Journal of Physiology-Cell Physiology* **2019**, *316* (5), C583–C604. https://doi.org/10.1152/ajpcell.00523.2018.
(160) Xie, L.; Shi, F.; Li, Y.; Li, W.; Yu, X.; Zhao, L.; Zhou, M.; Hu, J.; Luo, X.; Tang, M.; Fan, J.; Zhou, J.; Gao, Q.; Wu, W.; Zhang, X.; Liao, W.; Bode, A. M.; Cao, Y. Drp1-Dependent Remodeling of Mitochondrial Morphology Triggered by EBV-LMP1 Increases Cisplatin

Resistance. *Sig Transduct Target Ther* **2020**, *5* (1), 1–12. https://doi.org/10.1038/s41392-020-0151-9.
(161) Kashatus, D. F. The Regulation of Tumor Cell Physiology by Mitochondrial Dynamics. *Biochemical and Biophysical Research Communications* **2018**, *500* (1), 9–16. https://doi.org/10.1016/j.bbrc.2017.06.192.
(162) Pernas, L.; Scorrano, L. Mito-Morphosis: Mitochondrial Fusion, Fission, and Cristae Remodeling as Key Mediators of Cellular Function. *Annual Review of Physiology* **2016**, *78* (Volume 78, 2016), 505–531. https://doi.org/10.1146/annurev-physiol-021115-105011.
(163) Chen, H.; Chomyn, A.; Chan, D. C. Disruption of Fusion Results in Mitochondrial Heterogeneity and Dysfunction *. *Journal of Biological Chemistry* **2005**, *280* (28), 26185–26192. https://doi.org/10.1074/jbc.M503062200.
(164) Liu, X.; Sun, J.; Yuan, P.; Shou, K.; Zhou, Y.; Gao, W.; She, J.; Hu, J.; Yang, J.; Yang, J. Mfn2 Inhibits Proliferation and Cell-Cycle in Hela Cells via Ras-NF-κB Signal Pathway. *Cancer Cell International* **2019**, *19* (1), 197. https://doi.org/10.1186/s12935-019-0916-9.
(165) Irazoki, A.; Gordaliza-Alaguero, I.; Frank, E.; Giakoumakis, N. N.; Seco, J.; Palacín, M.; Gumà, A.; Sylow, L.; Sebastián, D.; Zorzano, A. Disruption of Mitochondrial Dynamics Triggers Muscle Inflammation through Interorganellar Contacts and Mitochondrial DNA Mislocation. *Nat Commun* **2023**, *14* (1), 108. https://doi.org/10.1038/s41467-022-35732-1.
(166) Rahn, J. J.; Stackley, K. D.; Chan, S. S. L. Opa1 Is Required for Proper Mitochondrial Metabolism in Early Development. *PLOS ONE* **2013**, *8* (3), e59218. https://doi.org/10.1371/journal.pone.0059218.
(167) Davies, V. J.; Hollins, A. J.; Piechota, M. J.; Yip, W.; Davies, J. R.; White, K. E.; Nicols, P. P.; Boulton, M. E.; Votruba, M. Opa1 Deficiency in a Mouse Model of Autosomal Dominant Optic Atrophy Impairs Mitochondrial Morphology, Optic Nerve Structure and Visual Function. *Human Molecular Genetics* **2007**, *16* (11), 1307–1318. https://doi.org/10.1093/hmg/ddm079.
(168) Ishihara, N.; Nomura, M.; Jofuku, A.; Kato, H.; Suzuki, S. O.; Masuda, K.; Otera, H.; Nakanishi, Y.; Nonaka, I.; Goto, Y.; Taguchi, N.; Morinaga, H.; Maeda, M.; Takayanagi, R.; Yokota, S.; Mihara, K. Mitochondrial Fission Factor Drp1 Is Essential for Embryonic Development and Synapse Formation in Mice. *Nat Cell Biol* **2009**, *11* (8), 958–966. https://doi.org/10.1038/ncb1907.
(169) Hong, X.; Isern, J.; Campanario, S.; Perdiguero, E.; Ramírez-Pardo, I.; Segalés, J.; Hernansanz-Agustín, P.; Curtabbi, A.; Deryagin, O.; Pollán, A.; González-Reyes, J. A.; Villalba, J. M.; Sandri, M.; Serrano, A. L.; Enríquez, J. A.; Muñoz-Cánoves, P. Mitochondrial Dynamics Maintain Muscle Stem Cell Regenerative Competence throughout Adult Life by Regulating Metabolism and Mitophagy. *Cell Stem Cell* **2022**, *29* (9), 1298-1314.e10. https://doi.org/10.1016/j.stem.2022.07.009.
(170) Rocheteau, P.; Gayraud-Morel, B.; Siegl-Cachedenier, I.; Blasco, M. A.; Tajbakhsh, S. A Subpopulation of Adult Skeletal Muscle Stem Cells Retains All Template DNA Strands after Cell Division. *Cell* **2012**, *148* (1), 112–125. https://doi.org/10.1016/j.cell.2011.11.049.
(171) Forni, M. F.; Peloggia, J.; Trudeau, K.; Shirihai, O.; Kowaltowski, A. J. Murine Mesenchymal Stem Cell Commitment to Differentiation Is Regulated by Mitochondrial Dynamics. *Stem Cells* **2016**, *34* (3), 743–755. https://doi.org/10.1002/stem.2248.
(172) Buck, M. D.; O'Sullivan, D.; Klein Geltink, R. I.; Curtis, J. D.; Chang, C.-H.; Sanin, D. E.; Qiu, J.; Kretz, O.; Braas, D.; van der Windt, G. J. W.; Chen, Q.; Huang, S. C.-C.; O'Neill, C. M.; Edelson, B. T.; Pearce, E. J.; Sesaki, H.; Huber, T. B.; Rambold, A. S.;

Pearce, E. L. Mitochondrial Dynamics Controls T Cell Fate through Metabolic Programming. *Cell* **2016**, *166* (1), 63–76. https://doi.org/10.1016/j.cell.2016.05.035.
(173) Khacho, M.; Clark, A.; Svoboda, D. S.; Azzi, J.; MacLaurin, J. G.; Meghaizel, C.; Sesaki, H.; Lagace, D. C.; Germain, M.; Harper, M.-E.; Park, D. S.; Slack, R. S. Mitochondrial Dynamics Impacts Stem Cell Identity and Fate Decisions by Regulating a Nuclear Transcriptional Program. *Cell Stem Cell* **2016**, *19* (2), 232–247. https://doi.org/10.1016/j.stem.2016.04.015.
(174) Passos, J. F.; Saretzki, G.; Ahmed, S.; Nelson, G.; Richter, T.; Peters, H.; Wappler, I.; Birket, M. J.; Harold, G.; Schaeuble, K.; Birch-Machin, M. A.; Kirkwood, T. B. L.; Zglinicki, T. von. Mitochondrial Dysfunction Accounts for the Stochastic Heterogeneity in Telomere-Dependent Senescence. *PLOS Biology* **2007**, *5* (5), e110. https://doi.org/10.1371/journal.pbio.0050110.
(175) Yucel, N.; Wang, Y. X.; Mai, T.; Porpiglia, E.; Lund, P. J.; Markov, G.; Garcia, B. A.; Bendall, S. C.; Angelo, M.; Blau, H. M. Glucose Metabolism Drives Histone Acetylation Landscape Transitions That Dictate Muscle Stem Cell Function. *Cell Reports* **2019**, *27* (13), 3939-3955.e6. https://doi.org/10.1016/j.celrep.2019.05.092.
(176) Rampalli, S.; Li, L.; Mak, E.; Ge, K.; Brand, M.; Tapscott, S. J.; Dilworth, F. J. P38 MAPK Signaling Regulates Recruitment of Ash2L-Containing Methyltransferase Complexes to Specific Genes during Differentiation. *Nat Struct Mol Biol* **2007**, *14* (12), 1150–1156. https://doi.org/10.1038/nsmb1316.
(177) Cencioni, C.; Heid, J.; Krepelova, A.; Rasa, S. M. M.; Kuenne, C.; Guenther, S.; Baumgart, M.; Cellerino, A.; Neri, F.; Spallotta, F.; Gaetano, C. Aging Triggers H3K27 Trimethylation Hoarding in the Chromatin of Nothobranchius Furzeri Skeletal Muscle. *Cells* **2019**, *8* (10), 1169. https://doi.org/10.3390/cells8101169.
(178) Benayoun, B. A.; Pollina, E. A.; Singh, P. P.; Mahmoudi, S.; Harel, I.; Casey, K. M.; Dulken, B. W.; Kundaje, A.; Brunet, A. Remodeling of Epigenome and Transcriptome Landscapes with Aging in Mice Reveals Widespread Induction of Inflammatory Responses. *Genome Res.* **2019**, *29* (4), 697–709. https://doi.org/10.1101/gr.240093.118.
(179) Coppé, J.-P.; Desprez, P.-Y.; Krtolica, A.; Campisi, J. The Senescence-Associated Secretory Phenotype: The Dark Side of Tumor Suppression. *Annual Review of Pathology: Mechanisms of Disease* **2010**, *5* (Volume 5, 2010), 99–118. https://doi.org/10.1146/annurev-pathol-121808-102144.
(180) Tezze, C.; Romanello, V.; Desbats, M. A.; Fadini, G. P.; Albiero, M.; Favaro, G.; Ciciliot, S.; Soriano, M. E.; Morbidoni, V.; Cerqua, C.; Loefler, S.; Kern, H.; Franceschi, C.; Salvioli, S.; Conte, M.; Blaauw, B.; Zampieri, S.; Salviati, L.; Scorrano, L.; Sandri, M. Age-Associated Loss of OPA1 in Muscle Impacts Muscle Mass, Metabolic Homeostasis, Systemic Inflammation, and Epithelial Senescence. *Cell Metab* **2017**, *25* (6), 1374-1389.e6. https://doi.org/10.1016/j.cmet.2017.04.021.
(181) Joseph, A.-M.; Adhihetty, P. J.; Buford, T. W.; Wohlgemuth, S. E.; Lees, H. A.; Nguyen, L. M.-D.; Aranda, J. M.; Sandesara, B. D.; Pahor, M.; Manini, T. M.; Marzetti, E.; Leeuwenburgh, C. The Impact of Aging on Mitochondrial Function and Biogenesis Pathways in Skeletal Muscle of Sedentary High- and Low-Functioning Elderly Individuals. *Aging Cell* **2012**, *11* (5), 801–809. https://doi.org/10.1111/j.1474-9726.2012.00844.x.
(182) Song, M.; Franco, A.; Fleischer, J. A.; Zhang, L.; Dorn, G. W. Abrogating Mitochondrial Dynamics in Mouse Hearts Accelerates Mitochondrial Senescence. *Cell Metabolism* **2017**, *26* (6), 872-883.e5. https://doi.org/10.1016/j.cmet.2017.09.023.

(183) Amartuvshin, O.; Lin, C.-H.; Hsu, S.-C.; Kao, S.-H.; Chen, A.; Tang, W.-C.; Chou, H.-L.; Chang, D.-L.; Hsu, Y.-Y.; Hsiao, B.-S.; Rastegari, E.; Lin, K.-Y.; Wang, Y.-T.; Yao, C.-K.; Chen, G.-C.; Chen, B.-C.; Hsu, H.-J. Aging Shifts Mitochondrial Dynamics toward Fission to Promote Germline Stem Cell Loss. *Aging Cell* **2020**, *19* (8), e13191. https://doi.org/10.1111/acel.13191.

(184) Balajee, A. S.; Geard, C. R. Replication Protein A and γ-H2AX Foci Assembly Is Triggered by Cellular Response to DNA Double-Strand Breaks. *Experimental Cell Research* **2004**, *300* (2), 320–334. https://doi.org/10.1016/j.yexcr.2004.07.022.

(185) Oizumi, T.; Suzuki, T.; Kobayashi, J.; Nakamura, A. J. Senescence-Associated Heterochromatin Foci Suppress γ-H2AX Focus Formation Induced by Radiation Exposure. *Int J Mol Sci* **2024**, *25* (6), 3355. https://doi.org/10.3390/ijms25063355.

(186) Del Toro, N.; Fernandez-Ruiz, A.; Mignacca, L.; Kalegari, P.; Rowell, M.-C.; Igelmann, S.; Saint-Germain, E.; Benfdil, M.; Lopes-Paciencia, S.; Brakier-Gingras, L.; Bourdeau, V.; Ferbeyre, G.; Lessard, F. Ribosomal Protein RPL22/eL22 Regulates the Cell Cycle by Acting as an Inhibitor of the CDK4-Cyclin D Complex. *Cell Cycle* **2019**, *18* (6–7), 759–770. https://doi.org/10.1080/15384101.2019.1593708.

(187) Redon, C. E.; Nakamura, A. J.; Sordet, O.; Dickey, J. S.; Gouliaeva, K.; Tabb, B.; Lawrence, S.; Kinders, R. J.; Bonner, W. M.; Sedelnikova, O. A. γ-H2AX Detection in Peripheral Blood Lymphocytes, Splenocytes, Bone Marrow, Xenografts, and Skin. In *DNA Damage Detection In Situ, Ex Vivo, and In Vivo: Methods and Protocols*; Didenko, V. V., Ed.; Humana Press: Totowa, NJ, 2011; pp 249–270. https://doi.org/10.1007/978-1-60327-409-8_18.

(188) Sharma, A.; Singh, K.; Almasan, A. Histone H2AX Phosphorylation: A Marker for DNA Damage. In *DNA Repair Protocols*; Bjergbæk, L., Ed.; Humana Press: Totowa, NJ, 2012; pp 613–626. https://doi.org/10.1007/978-1-61779-998-3_40.

(189) *Proteome Oxidative Modifications and Impairment of Specific Metabolic Pathways During Cellular Senescence and Aging - Hamon - 2020 - PROTEOMICS - Wiley Online Library*. https://analyticalsciencejournals.onlinelibrary.wiley.com/doi/10.1002/pmic.201800421 (accessed 2025-01-16).

(190) Frasca, D.; Saada, Y. B.; Garcia, D.; Friguet, B. Effects of Cellular Senescence on Metabolic Pathways in Non-Immune and Immune Cells. *Mechanisms of Ageing and Development* **2021**, *194*, 111428. https://doi.org/10.1016/j.mad.2020.111428.

(191) Fernandez-Rebollo, E.; Franzen, J.; Goetzke, R.; Hollmann, J.; Ostrowska, A.; Oliverio, M.; Sieben, T.; Rath, B.; Kornfeld, J.-W.; Wagner, W. Senescence-Associated Metabolomic Phenotype in Primary and iPSC-Derived Mesenchymal Stromal Cells. *Stem Cell Reports* **2020**, *14* (2), 201–209. https://doi.org/10.1016/j.stemcr.2019.12.012.

(192) James, E. L.; Lane, J. A. E.; Michalek, R. D.; Karoly, E. D.; Parkinson, E. K. Replicatively Senescent Human Fibroblasts Reveal a Distinct Intracellular Metabolic Profile with Alterations in NAD+ and Nicotinamide Metabolism. *Sci Rep* **2016**, *6* (1), 38489. https://doi.org/10.1038/srep38489.

(193) Hetz, C.; Zhang, K.; Kaufman, R. J. Mechanisms, Regulation and Functions of the Unfolded Protein Response. *Nat Rev Mol Cell Biol* **2020**, *21* (8), 421–438. https://doi.org/10.1038/s41580-020-0250-z.

(194) Hetz, C. The Unfolded Protein Response: Controlling Cell Fate Decisions under ER Stress and Beyond. *Nat Rev Mol Cell Biol* **2012**, *13* (2), 89–102. https://doi.org/10.1038/nrm3270.
(195) Harding, H. P.; Zhang, Y.; Zeng, H.; Novoa, I.; Lu, P. D.; Calfon, M.; Sadri, N.; Yun, C.; Popko, B.; Paules, R.; Stojdl, D. F.; Bell, J. C.; Hettmann, T.; Leiden, J. M.; Ron, D. An Integrated Stress Response Regulates Amino Acid Metabolism and Resistance to Oxidative Stress. *Molecular Cell* **2003**, *11* (3), 619–633. https://doi.org/10.1016/S1097-2765(03)00105-9.
(196) Katsiki, M.; Chondrogianni, N.; Chinou, I.; Rivett, A. J.; Gonos, E. S. The Olive Constituent Oleuropein Exhibits Proteasome Stimulatory Properties In Vitro and Confers Life Span Extension of Human Embryonic Fibroblasts. *Rejuvenation Research* **2007**, *10* (2), 157–172. https://doi.org/10.1089/rej.2006.0513.
(197) Cormenier, J.; Martin, N.; Deslé, J.; Salazar-Cardozo, C.; Pourtier, A.; Abbadie, C.; Pluquet, O. The ATF6α Arm of the Unfolded Protein Response Mediates Replicative Senescence in Human Fibroblasts through a COX2/Prostaglandin E2 Intracrine Pathway. *Mechanisms of Ageing and Development* **2018**, *170*, 82–91. https://doi.org/10.1016/j.mad.2017.08.003.
(198) Fu, X.; Wang, H.; Hu, P. Stem Cell Activation in Skeletal Muscle Regeneration. *Cell. Mol. Life Sci.* **2015**, *72* (9), 1663–1677. https://doi.org/10.1007/s00018-014-1819-5.
(199) Brun, C. E.; Wang, Y. X.; Rudnicki, M. A. Single EDL Myofiber Isolation for Analyses of Quiescent and Activated Muscle Stem Cells. In *Cellular Quiescence: Methods and Protocols*; Lacorazza, H. D., Ed.; Springer: New York, NY, 2018; pp 149–159. https://doi.org/10.1007/978-1-4939-7371-2_11.